NATIONAL ADVISORY COMMITTEE FOR AERONAUTICS

TECHNICAL MEMORANDUM

No. 1113

INVESTIGATIONS OF COMPRESSION SHOCKS AND BOUNDARY LAYERS IN GASES MOVING AT HIGH SPEED

By J. Ackeret, F. Feldmann, and N. Rott

Translation

"Untersuchungen an Verdichtungsstössen und Grenzschichten in schnell bewegten Gasen." Mitteilungen aus dem Institut für Aerodynamik an der Eidgenössischen Technischen Hochschule in Zürich Herausgegeben von Prof. Dr. J. Ackeret, No. 10.

Washington
January 1947

NATIONAL ADVISORY COMMITTEE FOR AERONAUTICS

TECHNICAL MEMORANDUM NO. 1113

INVESTIGATIONS OF COMPRESSION SHOCKS AND BOUNDARY LAYERS IN GASES MOVING AT HIGH SPEED*

By J. Ackeret, F. Feldmann, and N. Rott

INTRODUCTION

It has been known for some time that at high flight velocities marked increases in drag coefficient occur. The flight velocity V is measured in terms of the speed of sound as by the Mach number $M = \frac{V}{a}$. For wing profiles of usual thickness the increase starts at $M = 0.75$ to 0.85 and the maximum drag coefficients measured become about 10 times the normal values.

A more thorough investigation shows that the drag increase is connected with large changes in the pressure distribution so that the increase is caused by the normal pressures rather than by skin friction. The chordwise pressure distribution (fig. 8) for large M shows an extensive low-pressure region on the upper surface of the wing where, local velocities considerably exceed sonic velocity, followed by a sudden pressure jump; whereas such jumps are not noticed for smaller Mach numbers, for which sonic velocity is nowhere exceeded.

It has been known for some time that these jumps are merely Riemann's compression shocks which cause a discontinuous transition from supersonic to subsonic velocity.

Unfortunately, there is no prospect of a possibility of calculating these phenomena on the profile in advance, since one has to deal with differential equations which undergo basic changes in character at the (a priori unknown) boundary between the subsonic and supersonic regions.

---

*"Untersuchungen an Verdichtungsstössen und Grenzschichten in schnell bewegten Gasen." Mitteilungen aus dem Institut für Aerodynamik an der Eidgenössischen Technischen Hochschule in Zürich Herausgegeben von Prof. Dr. J. Ackeret, No. 10.

It is the purpose of the following investigation to examine experimentally more closely the mutual influences of the compression shocks and the friction boundary layers. A comparison of measurements taken in various high-speed wind tunnels has shown that not always does the same shock picture appear. It was to be suspected that friction effects are of importance here, which have to be clarified, and the experimental results showed, in fact, that the shock picture is different for a laminar than for a turbulent boundary layer - for the laminar case the shock pattern is much more complicated. The problem is of practical importance because of effort to achieve low drag by means of extensive laminar boundary layers. The tests were made in the high-speed wind tunnel of the institute.[1] This tunnel has the great advantage of permitting the determination of the Mach number and the Reynolds number effects separately, through provision for varying the density of the gas at constant velocity. Only this separation of the effects made it possible to disentangle the phenomena somewhat satisfactorily.

APPARATUS AND TESTS

A. Test Setup

The test section consists essentially of a nozzle with a curved axis. (See fig. 1.) Its cross section is everywhere rectangular and of uniform width. A portion of the lower wall of the nozzle is shaped like a wing surface. The upper wall of the nozzle was arranged so that it corresponded approximately to the course of a streamline of the flow about the wing. The whole upper wall of the nozzle is flexible and can be adjusted during the operation. Because of the curvature of the lower wall of the nozzle a supersonic region develops over it at certain free-stream velocities.

The tests were carried out in such a manner that sonic velocity was not reached over the whole nozzle cross section. Therefore a local supersonic region is obtained which does not reach the upper wall of the nozzle at any point. Because of an increased cross section immediately downstream of this region, a compression takes place, which gives rise to the compression shock. The nozzle then contracts again to the minimum cross section. As is known, exactly sonic velocity will appear at this minimum cross

---

[1] J. Ackeret, The Institute for Aerodynamics at the Federal Academy for Technology. ("Das Institut für Aerodynamik an der Eidgenössischen Technischen Hochschule.") Mitteilungen aus dem Institut für Aerodynamik No. 8, Zürich 1943.

section when the critical pressure ratio is reached. The maximum mass flow is, for constant initial conditions, proportional to the minimum cross section; hence, the air velocity and therefore the local Mach numbers can be simply regulated by changing the minimum cross section. There was always sufficient power expended so that sonic velocity was reached at the minimum cross section. Transmission of pressure disturbances from the following diffuser upstream into the test section was thereby prevented. It proved advantageous, in order to maintain a constant position of the compression shock, to break off the lower wall of the nozzle immediately behind the minimum cross section and to let the flow expand around the resulting sharp edge.

For test series I to VI a plate parallel to the lower nozzle wall was placed at a distance of 40 millimeters above it; a new boundary layer developed at the leading edge of this plate and the thick turbulent boundary layer along the tunnel wall could flow between the auxiliary plate and the wall of the nozzle. Thereby, in a certain range of Reynolds numbers (corresponding to different adjustments of the pressure) either laminar or turbulent boundary layers ahead of the compression shock could be produced.

For test series VII this auxiliary plate was removed so that the investigation could be carried out with a thick turbulent boundary layer.

B. Test Instruments

(a) Schlieren optics

The schlieren apparatus used has been described before.[2] It works according to the principle of the coincidence method[3]; the path of the rays can be seen in figure 2. A Philips Philora high-pressure-mercury vapor lamp was used as the light source. The schlieren knife-edge itself can be rotated so that pressure gradients in all directions of the flow field can be made visible. The position of the glass window is indicated in figure 1. The field of vision has a diameter of 250 millimeters. The light rays

---

[2] P. de Haller, The Schlieren Optics of the Supersonic Tunnel. ("Die Schlierenoptik des Überschallkanales.") Mitteilungen aus dem Institut für Aerodynamik, No. 8, Zurich 1943.

[3] H. Schardin, Schlieren Methods and their Applications. ("Schlierenverfahren und ihre Anwendungen.") Ergebnisse der exakten Naturwissenschaften, Vol. 20. Springer 1942. pp. 303-439.

are transmitted through the tunnel walls by means of 25-millimeter-thick glass plates ground plane parallel. The rays are reflected by a concave mirror mounted outside of the tunnel, having a silvered surface and a 3000-millimeter focal length. The image is projected onto a ground glass or a screen. The photographs were taken by means of a miniature camera on Leicafilm. The light intensity was sufficient to obtain high sensitivity with film of normal speed and exposure times of 1/250 to 1/500 second, with most of the light blanked off by the knife-edge. These exposure times proved to be sufficiently short to produce sharp photographs even with somewhat unsteady compression shocks. Because of the conical-ray path, straight lines located outside of the optic axis and parallel to it do not appear as points; therefore the compression shocks were as far as possible adjusted so as to be in the proximity of the optic axis.

The schlieren photographs gave a clear picture of the flow phenomena and were used for determination of the location of the compression shocks, for measurement of shock angles and also of Mach angles for determining the velocity.

(b) Pressure measurements

The measurement of the static pressure at the wall, particularly at the plate surfaces in the domain of the compression shocks is made by means of holes of 0.3-millimeter diameter. For instance, 36 test holes were provided on the auxiliary plate. The distribution of the static pressure in the flow itself was ascertained by means of static-pressure probes. (See fig. 3.) The mechanism which permits adjustment of these static-pressure probes in the x-direction and the z-direction (fig. 1) is electrically operated. The local disturbance of the flow was small due to the smallness of the static-pressure probes.

Total-pressure tubes with an electrically operated adjustment mechanism were also used for measurement of the total pressure. (See fig. 3.) The boundary-layer measurements were made by means of a very thin curved total-pressure tube, the dimensions of which can be seen in figure 3. Thus the total pressure could be measured up to 0.3-millimeter distance from the wall.

The pressures were measured with a mercury-micromanometer; small differences in pressure were determined by means of an alcohol manometer. The accuracy of the readings was 1/10-millimeter mercury and alcohol, respectively.

(c) Determination of the humidity of air

The air humidity was measured with a dry-bulb and a wet-bulb thermometer in the large cross section behind the straightening vanes where the air velocities are small. The humidity in other places can then be calculated from knowledge of the local state of the air.

C. Method of Measurement

Initially there were difficulties regarding the reproducibility of the compression shocks. Due to various influences, for instance; dilatations of the tunnel walls by heating, changes in cross section appeared which affected the position of the compression shock. Therefore a photographic negative of each investigated compression shock was made and the pressure distribution on the surface of the plate was measured. To reproduce a certain compression shock the pressure in the tunnel was first adjusted and the temperature regulated by varying the cooling water supply. After steady conditions were established (which can be ascertained by means of a variometer) the position of the shock was adjusted, with the aid of the negative and the measured pressure distribution, by varying the minimum nozzle cross section. Measurements could then be continued as long as necessary without any noticeable change in the flow condition in the tunnel.

SYMBOLS AND BASIC EQUATIONS

1. Symbols and Dimensions

p	absolute static pressure, kilograms per meter^2
p_o	stagnation pressure, kilograms per meter^2
p_p	pressure at rest measured with pitot tube, kilograms per meter^2
p^*	critical pressure, kilograms per meter^2
T	absolute temperature, °Kelvin
T_o	absolute stagnation temperature, °Kelvin
ρ	air density, kilogram-second^2 meter^4
γ	specific weight ($= g\rho$), kilograms per meter^3
η	viscosity of air, kilogram-second per meter^2
υ	kinematic viscosity, $\left(= \frac{\eta}{\rho}\right)$ meters^2 per second
w	air velocity, meters per second
U	air velocity outside of the boundary layer, meters per second
a	sonic velocity (local), meters per second

a^* critical sonic velocity, meters per second

M Mach number (local)

M^* Mach number (referred to a^*)

c_p, c_v specific heats, (k Cal/kg°)

k $c_p/c_v = 1.4$ for air

R gas constant = 29.27 for dry air, meters per degree

A mechanical heat equivalent = 1/427, (k Cal/mkg)

δ thickness of the boundary layer

δ^* displacement thickness, δ^{**} momentum thickness } equations (10) and (11)

φ direction of the schlieren knife-edge vertical

θ direction of the schlieren knife-edge horizontal

$\longrightarrow$ direction of flow

The positions of the points of measurement were referred to the coordinate system x, z shown in figure 1.

2. The Reynolds Numbers

For comparison of the tests the following two Reynolds numbers were introduced:

(a) Reynolds number for the tests with auxiliary plate: $Re_l = \frac{Ul}{\upsilon}$

with U and υ representing the local values for the point x = 106.5 millimeters immediately outside of the boundary layer. l is length of the auxiliary plate = 0.55 meter.

(b) $Re_\delta^{**} = \frac{U\delta^{**}}{\upsilon}$: Reynolds number formed from the undisturbed velocity, the corresponding kinematic viscosity and the boundary-layer momentum thickness immediately ahead of the first compression shock.

3. The Mach Numbers

The Mach numbers given for the separate test series are the local values immediately ahead of the first compression shock at the distance of the boundary-layer thickness from the wall surface.

4. Determination of Velocity, Temperature, and Density

The static pressure p and the pitot pressure p_p were measured at every test point. For subsonic flow p_p equals the stagnation pressure p_o which is obtained through adiabatic compression to zero velocity. For supersonic flow the compression occurs partially through a normal shock, thus not adiabatically. Therefore one obtains according to whether the local Mach number M is smaller or larger than 1:[4]

$$M \leq 1: \quad \frac{p_p}{p} = \frac{p_o}{p} = \left(1 + \frac{k-1}{2}M^2\right)^{\frac{k}{k-1}} \tag{1}$$

$$M \geq 1: \quad \frac{p_p}{p} = \frac{k+1}{2}M^2\left[\frac{(k+1)^2M^2}{4kM^2 - 2(k-1)}\right]^{\frac{1}{k-1}} \tag{2}$$

The two curves given by the above formulas meet for $M = 1$ with continuous tangent and curvature. Formula (1) or (2) is used according to whether the ratio p/p_p is larger or smaller than the critical pressure ratio:

$$\left(\frac{p}{p_p}\right)_{crit.} = \frac{p^*}{p_p} = \left(\frac{2}{k+1}\right)^{\frac{k}{k-1}} = 0.5283 \quad (\text{for } k = 1.4)$$

---

[4] R. Sauer, Gas Dynamics ("Gasdynamik.") Springer 1943, pp. 8 and 79.

The relation (1) can be solved for M:

$$M^2 = \frac{2}{k-1}\left[\left(\frac{p_o}{p}\right)^{\frac{k-1}{k}} - 1\right] \qquad (1(a))$$

whereas for equation (2) an interpolation has to be used.

For stagnation of the flow, (no heat added or removed)

$$\frac{Aw^2}{2g} + c_pT = c_pT_o \qquad (3)$$

where T_o is the stagnation temperature. By transformation there follows from it:

$$w^2 = gkRT_o \frac{M^2}{1 + \frac{k-1}{2}M^2} = a_o^2 \frac{M^2}{1 + \frac{k-1}{2}M^2} \qquad (4)$$

Thus one can obtain the local Mach number M according to (1) or (2) from p and p_p alone whereas for determination of w according to (4) the stagnation temperature T_o must also be known.

In the present tests T_o was measured at a single place (at small velocity). T_o remains constant in adiabatic flow and through shocks so that this measurement is sufficient for determinations of velocity outside of the boundary layer.

According to Busemann[5] the stagnation temperature T_o is also constant everywhere in the boundary layer, if the boundary layer is

---

[5] A. Busemann, Gas Dynamics, in "Handbook of Experimental Physics" ("Gasdynamik," in "Handbuch der Experimentalphysik") of Wien-Harms, Vol. IV, 1, p. 365, Leipzig 1931.- Compare also A. Stodola, Contributions to the Theory of the Heat Transfer of Liquids or Gases to Solid Walls, ("Zur Theorie des Wärmeüberganges von Flüssigkeiten oder Gasen an feste Wände"), Schweiz. Bauzeitung, Vol. 88, p. 243, 1926.

turbulent: if it is laminar T_o = constant is valid only when the Prandtl number $\sigma = \frac{\eta g c_p}{\lambda}$ equals 1. In both cases one has to presume that heat is neither added nor escaping through the wall, which should be true for the present tests. For air, however, σ does not equal exactly 1 ($\sigma \approx 0.7$). Pohlhausen[6] investigated by calculation the deviations from T_o = constant in the laminar boundary layer which originate because of $\sigma \neq 1$. It appears that the influence of $\sigma \neq 1$ for air upon the determination of velocity in the laminar boundary layer is slight. For simplification, all calculations therefore were made for T_o = constant.

With the assumption T_o = constant within and outside of the boundary layer there follows from (3) the temperature T at any point:

$$\frac{T_o}{T} = 1 + \frac{k-1}{2} M^2 \tag{5}$$

Finally, the density results from the equation of state

$$\rho = \frac{p}{gRT} \tag{6}$$

5. The Boundary Layer for Compressible Flow

The momentum equation of the boundary layer

$$U\frac{d}{dx}\int_0^\delta \rho w \, dy - \frac{d}{dx}\int_0^\delta \rho w^2 \, dy - \delta\frac{dp}{dx} = \tau_o \tag{7}$$

---

[6] E. Pohlhausen, The Heat Exchange between Solid Bodies and Liquids with Small Friction and Small Heat Transfer. ("Der Wärmeaustausch zwischen festen Körpern und Flüssigkeiten mit kleiner Reibung und kleiner Wärmeleitung") Z.A.M.M., Vol. 1, pp. 115-121, 1921. More recent authors consider also the influence of the pressure gradient outside of the boundary layer upon the temperature distribution; compare for instance, A. N. Tifford, Journal of the Aeronautical Sciences, Vol. 12, p. 241, 1945, where further references can be found.

is also valid in the above form for compressible flow. For the flow outside of the boundary layer the differential form of Bernoulli's equation is valid; thus

$$\frac{dp}{dx} = -\frac{\rho_u}{2}\frac{dU^2}{dx} \tag{8}$$

with ρ_U representing the density at the edge of the boundary layer. One can write the boundary-layer momentum equation (7) also for compressible flow in Gruschwitz'[7] form with the aid of (8) and using the identity

$$\delta = \int_0^{\delta} dy$$

However, ρ will not be constant in the boundary layer for this case, and ρ_U will be a function of x. There results

$$\frac{d\delta^{**}}{dx} + \frac{1}{\rho_u U^2}\frac{d(\rho_u U^2)}{dx}\delta^{**} + \frac{1}{U}\frac{dU}{dx}\delta^{*} = \frac{\tau_o}{\rho_u U^2} \tag{9}$$

where δ^* is the displacement thickness:

$$\delta^* = \int_0^{\delta}\left(1 - \frac{\rho}{\rho_u}\frac{w}{U}\right)dy \tag{10}$$

and δ^{**} the momentum thickness

$$\delta^{**} = \int_0^{\delta}\frac{\rho}{\rho_u}\frac{w}{U}\left(1 - \frac{w}{U}\right)dy \tag{11}$$

---

[7]E. Gruschwitz, The Turbulent Friction Layer in Two-Dimensional flow ("Die turbulente Reibungsschicht in ebener Strömung"). Ingenieur-Archiv, Vol. 2, p. 321, 1931.

For $\rho = \rho_U$ = constant one obtains again the known equation and the former definition of δ^* and δ^{**} for incompressible flow.

Displacement thickness and momentum thickness were calculated according to the formulas (10) and (11); a determination of the shear stress at the wall τ_o with the aid of equation (9) was also attempted.

TEST RESULTS

Test Series I

The characteristic data of the flow are:

$M = 1.225$

$Re_l = 1.325 \times 10^6$

$Re_\delta{}^{**} = 400$

} Measured immediately ahead of the first compression shock

Boundary layer ahead of the shock: laminar

Because of its shape the compression shock investigated in this test series was designated with the Greek λ. (See fig. 4.)

Compression shocks of a similar nature also were observed in other tests, for instance, in de Haller's investigation of wings[8].

A. The pressure field

The measured distribution of the static pressure at various distances from the wall is shown in figure 5, in which the curves $p/p_o = f(x)_z$ are plotted. The critical-pressure ratio p^*/p_o for which exactly sonic velocity exists was drawn in a dash-dotted line.

---

[8] P. de Haller, l.c. p. 44.

The pressure field gives information about the extent of the supersonic region. The zone of supersonic velocity begins near the wall at $x \sim 72$ millimeters. The pressure distribution at the surface ($z = 0$ millimeters) shows a further decrease in pressure down to the point $x \sim 154$ millimeters where the lowest pressure is reached with $p/p_0 = 0.399$. The Mach number corresponding to this value is $M = 1.225$. Immediately afterwards there starts the oblique compression shock which can also be seen in the schlieren photograph. The pressure increase caused by it is relatively small; the pressure gradient dp/dx also is small. This behaviour can be seen also in the schlieren photograph.

The oblique compression shock can be further observed with the aid of the pressure measurements at the distances from the wall $z = 20$, 40, and 60 millimeters. At about $z = 80$ millimeters it meets the main shock.

Starting at $x \sim 205$ millimeters a further increase in pressure of large magnitude takes place on the plate surface. It amounts to about 36 percent of the maximum pressure drop. It is remarkable that this compression at the plate surface does not occur with a shock.

Outside of the boundary layer, at $x \sim 215$ millimeters the schlieren photograph and the pressure-distribution curves show a strong compression shock which leads to subsonic velocity. Boundary layer measurements demonstrate that this shock protrudes into the outer part of the friction layer as far as supersonic velocity exists. It should be noted that the schlieren photograph does not show the total boundary-layer thickness. The beginning of the darkening in the picture lies where a gradient in the temperature profile of the boundary layer appears and, consequently, the maximum air-density gradients occur. However, these dark areas lie, as shown by the measurements, within the boundary layer. Therefore, the friction layer is thicker than it appears in the schlieren photograph.

One must distinguish two zones in the boundary layer, one near the wall in which the velocity increases from 0 up to sonic velocity, and an adjoining one in which the velocity further increases up to the undisturbed supersonic velocity U. It is possible that compression shocks may occur in the outer thin zone of the boundary layer whereas the pressure increases in the inner layer take place continuously. As pressure measurements show, the intensity of the compression shock decreases on entering the outer zone of the boundary layer according to the decreasing velocities. In the subsonic zone of the friction layer near the wall the back pressure can be propagated upstream beyond the main

shock. Thereby a continuous pressure increase develops which starts ahead of the main shock and does not reach the pressure of the undisturbed flow until relatively far behind the main shock. From this fact there results within the boundary layer ahead of the compression shock a pressure drop toward the outside and behind the compression shock a pressure drop toward the inside. (See fig. 6.) The changes in density which thus originate are visible in the schlieren photograph of figure 4 in the shape of a black line starting at the oblique shock and inclined towards the surface.

With increasing distance from the wall the intensity of the main shock decreases, corresponding to the decreasing velocities. Where the velocity just reaches local sonic velocity the main shock is transformed into an adiabatic compression. Therefore, the entire supersonic region from the wall to its outer boundary goes over into a subsonic velocity region by means of the main shock. It is peculiar that a renewed expansion to supersonic velocity takes place after this compression shock between the boundary layer and a distance from the wall $z \sim 35$ millimeters, as is shown by the schlieren photograph and the pressure distribution curves. This small zone of supersonic velocity is bounded in the direction of the flow by a further small compression shock. It could not be clarified whether this second expansion is due to the behaviour of the boundary layer or to the curvature of the plate. The fact is that the expansion gradually disappears when the Mach number is increased and the main shock thereby shifted downstream. A simple proof for the reality of this second expansion "post expansion" (besides the pressure measurements and the strong brightening in the schlieren photograph) is the presence of Mach waves in this region caused by a small disturbance (pitot-tube tip). The Mach angles formed thereby give practically the same Mach number that can be calculated from the pressure measurements.

The entire pressure field may be represented by isobars. (See fig. 7.) One can see here clearly the relatively small pressure gradient and pressure rise in the oblique compression shock as compared to the much larger values of the main shock. The zone of supersonic velocity behind the main shock and also the following small compression shock are clearly visible. One can follow further the flattening of the steep pressure rise in the main shock through the boundary layer.

In addition it should be noted that the pressure measurements show rather good agreement with the schlieren photographs. Even small pressure gradients can be made visible as darkening or brightening if the direction of the schlieren knife-edge is favourable.

The pressure-distribution measurements by de Haller are mentioned for comparison with test series I. Figure 8 shows the compression shock on the upper side (0) of a wing of 10-percent thickness. The Mach number of the free-stream velocity is 0.818. The schlieren photograph of the compression shock and the pressure distribution measured at the surface show a similar behaviour similar to that found in test series I. Here again an oblique shock extends from the surface, which meets the main shock at a certain distance from the boundary. Behind the main shock a lightening of the schlieren photograph can also be ascertained outside of the boundary layer corresponding to a pressure reduction. Immediately following is another compression in the flow direction.

B. The boundary-layer behaviour

In order to investigate the mutual influence of compression shock and boundary layer, static and total pressures in the boundary layer were measured.

Several characteristic boundary-layer profiles are plotted in figure 9. The velocities, referred to the critical velocity a^*, as function of the distance from the wall z, are plotted. The displacement thickness calculated from these measurements can be seen from figure 10. The measurements indicate a laminar boundary layer ahead of the λ-shock. The Reynolds number at the point $x = 145$ millimeters, referred to the momentum thickness and the undisturbed flow velocity, is 440. From the point $x \sim 150$ millimeters, that is, from the starting point of the oblique shock, the boundary layer begins to thicken in the shape of a wedge. This phenomenon can also be seen in the schlieren photograph of figure 4. The velocity profiles pertaining to this wedge show reversed flow at the wall which displaces the laminar layer from the wall. The displacement thickness δ^* increases approximately linearly in this region.

The transition to turbulent boundary layer starts downstream, at about $x = 195$ millimeters. The boundary layer thickens considerably because of the pressure rise starting there. The displacement thickness δ^* increases between $x = 145$ millimeters and $x = 250$ millimeters to 10 times its value; the same holds true for the momentum thickness δ^{**}. Considerable variations with time of the total pressure can be noticed in this boundary layer during the tests, whereas the static pressure remains rather constant with time.

C. The oblique shock

For the oblique compression shock the following measurements were taken:

(a) The pressure rise Δp (by pressure measurement)

(b) The shock angle σ (taken from the schlieren photograph)

(c) The deflection angle δ (given by the course of the displacement thickness, thus by boundary-layer measurements)

The oblique compression shock is uniquely determined by one of these three dimensions together with the condition before the shock which is also known from measurements. Thus the possibility of several checks is obtained.

The basic equations of the compression shock[9] are transformed into the equation

$$\frac{\Delta p}{p_1} = \frac{2k}{k+1}(M_1^2 \sin^2\sigma - 1) \tag{12}$$

The subscript 1 refers to the condition before the shock. The equation (12) gives from the measured Δp, the value $\sigma = 54.8°$, which agrees very well with the shock angle in the schlieren photograph.

For the deflection angle δ one obtains from the continuity equation[9] (subscript 2: condition after the shock)

$$\frac{\rho_2}{\rho_1} = \frac{\tan\sigma}{\tan(\sigma - \delta)} \tag{13}$$

---

[9]For instance, R. Sauer, Gas Dynamics ("Gasdynamik.") Springer 1943, pp. 63-66.

which, together with Hugoniot's relation

$$\frac{\rho_2}{\rho_1} = \frac{1 + \frac{k+1}{k-1}\frac{p_2}{p_1}}{\frac{k+1}{k-1} + \frac{p_2}{p_1}} \tag{14}$$

makes the calculation of δ from the pressures and the shock angle possible. For the present case the result is $\delta = 1.9^\circ$. On the other hand a flow deflection of about 2° was ascertained due to the wedge shaped thickening of the boundary layer at the point $x \sim 145$ millimeters. This result also is a supporting fact for the assumption that the oblique compression shock at the λ-shock is an effect of the flow deflection by the boundary layer.

D. The shock losses

The λ-shock consists essentially of the main shock and the oblique compression shock. From the laws concerning the meeting of various shocks there follows that the streamline passing through the intersection of the main shock and the oblique compression shock contains a vortex layer in its downstream part[10]. The conditions that the velocity directions are parallel and that the same pressures exist hold for the regions immediately above and below the vortex layer. The velocity magnitudes are not equal due to unequal shock loss which is the reason for the formation of the vortex layer.

Since there results a shock intensity continuously varying with distance from the wall at the λ-shock, the shock loss is also variable, and the subsequent flow will therefore no longer be free of vortices.

The "total pressure loss" or "shock loss" $p_o - p_p$ was measured at the point $x = 261$ millimeters as a function of the distance from the wall. (See fig. 11.) Immediately above the

---

[10] E. Preiswerk, Application of Gas Dynamic Methods to Water Flows with Free Surface. ("Anwendung gasdynamischer Methoden auf Wasserströmungen mit freier Oberfläche.") Mitteilungen aus dem Institut für Aerodynamik, No. 7, Zürich 1938, p. 88.

surface there is a high total pressure loss as a result of the energy loss in the separated boundary layer. In the outer supersonic region of the friction layer a part of the shock loss is added. Outside of the boundary layer there exists only pure shock loss. Due to the compression in two stages this total pressure loss up to z = 80 millimeters is not as large as if the compression had taken place in a single compression shock. On the basis of this consideration the second maximum of the total pressure loss near z = 80 millimeters also is explained since from there on the compression takes place in one single strong shock. This pressure loss also is reduced toward the outside where the shock intensity is low. It is possible to calculate the shock losses from the distribution of the static pressure. The results thus obtained agree well with the experimental values outside of z = 80 millimeters; below z ~ 80 millimeters they are about six percent larger than the measured shock loss.

Test Series II

Characteristic data:

$Re_1 \sim 1.325 \times 10^6 \sim$ constant

M variable from 1.106 to 1.250

Boundary layer in front of the shock: laminar

In this test series the influence of the Mach number upon the λ-shock was investigated. The Reynolds number is approximately the same for all tests. As already mentioned, the variation of the Mach number was obtained by changing the minimum cross section at the end of the nozzle.

The schlieren photographs (fig. 12) show the remarkable phenomenon that for small Mach numbers several λ-shocks occur in succession. The extension of the successive shocks decreases in the flow direction.

For increasing Mach number the compression shocks increase corresponding to the growth of the supersonic velocity region. However, as the extention of the compression shocks increases their number decreases. There result for instance for:

M = 1.106 6 to 7 compression shocks

M = 1.204 2 compression shocks

M = 1.240 and beyond that number only 1 λ-shock

A. The pressure-distribution measurements

The most important measurements were the distribution of the static pressure at the plate surface. (See fig. 13.) First of all these pressure curves show that the compression in stages (corresponding to the multiple shocks) does not appear at the plate itself. The separate small unsteady pressure increases cannot exist in the subsonic velocity region of the boundary layer. A slight pressure rise in the flow direction takes place at the wall at the point where the first oblique compression shock outside of the laminar boundary layer occurs. Afterwards the pressure is almost constant for a short distance. Following this first rise a larger rise in pressure takes place. The second pressure rise starts slightly ahead of the last of the several λ-shocks and dies off some distance behind it. The gradient of the second compression increases visibly with decreasing Mach number. This increase is caused by the reduction of the thickening of the boundary layer at this point with decreasing Mach number and by the fact that the sonic speed boundary in the friction layer lies nearer to the surface of the plate.

For the Mach number $M = 1.191$ the pressure distribution was measured at the wall and at a distance of $z = 20$ millimeters. (See fig. 14.) At the surface of the plate there results the pressure distribution explained above, whereas at the distance $z = 20$ millimeters a pressure distribution was measured which corresponded to the schlieren photograph; that is, the separate pressure waves are clearly visible. At $z = 20$ millimeters, the first λ-shock causes a compression of $p/p_o = 0.48$ to 0.557, that is, a compression to subsonic velocity. Following it another expansion to supersonic velocity takes place. The pressure rise in the second λ-shock is smaller than in the first one and the following expansion just reaches sonic velocity. The third shock, together with the continuous compression following it, yield a pressure rise up to the back pressure. Analogous behaviour can be observed for other Mach numbers.

B. The behaviour of the boundary layer

Only a few boundary-layer profiles were included in this test series. In the region of the Mach numbers considered in this case around $M = 1$ the flow is very sensitive to changes in cross section. The insertion of a boundary-layer total pressure tube into the friction layer which is about 1 millimeter thick strongly influences the flow so that the results are not very reliable. However, the schlieren photographs permit various conclusions to be drawn; moreover, the behaviour of the boundary layer for the λ-shock at $M = 1.225$ is known. (See test series I.)

The schlieren photographs show that essentially a wedgelike thickening of the laminar boundary layer again develops. The wedge starts with the first oblique shock and extends in the direction of the flow to the subsonic region. The extent of the influence of the separate compression shocks and the expansions following them upon the boundary-layer thickness could not be determined. The length of the wedge increases somewhat with increasing Mach number.

The transition point of the boundary layer coincides rather accurately with the beginning of the steep pressure rise at the wall. In some cases a small expansion was observed in front of this pressure rise.

C. Similar observations

The investigations of wings by de Haller result in the same behaviour of the λ-shock for small Mach numbers.

Figure 15 shows the schlieren photograph and the pressure distribution of a wing for $\alpha = -1.6^{\circ}$ and $M = 0.845$ (of the free-stream velocity). Due to the negative angle of attack larger excess velocities originate on the lower side of the wing than on the upper side. The local Mach numbers immediately in front of the first shock are $M = 1.22$ below and $M = 1.16$ above. The λ-shocks are, in agreement with the results of test series II, larger but less numerous on the lower than on the upper side.

Test Series III

Characteristic data:

$M = 1.3225$

$Re_l = 2.63 \times 10^6$

$Re_\delta{}^{**} = 1478$

Boundary layer ahead of the shock: turbulent

The test conditions of the test series III are apart from the higher Reynolds number exactly the same as the conditions of test series I. In particular, the Mach numbers of the free-stream velocity with respect to the auxiliary plate are equal for both cases. Therefore, deviations in the results obtained are exclusively due to the change of the Reynolds number.

A comparison of the schlieren photograph obtained (fig. 16) with the one of the λ-shock from test series I shows two main characteristics. First of all, the oblique compression shock, located relatively far ahead of the main shock, is missing. Second, it is to be noted that the boundary layer is thickened to a much less degree by the compression shock.

A. The pressure measurements

The measurements of the static pressure were carried out in the same way as in test series I. The curves $p/p_o = f(x)_z$ can be seen from figure 17.

The flow expands at the surface of the plate to a point immediately in front of the main shock. Due to the lack of the oblique compression shock, therefore, larger excess velocities and correspondingly larger Mach numbers are reached ahead of the shock for the same free-stream velocity. The first part of the compression measured afterwards at the surface is considerably stronger than for the λ-shock; subsequently, however, its gradients become smaller. The pressure rise taking place at the wall amounts to about 41 percent of the maximum pressure gradient ahead of the shock. The pressure distributions in the flow direction for various distances from the wall result in very strong compressions through the compression shock. It must also be taken into consideration here that the strong gradients probably are slightly weakened at the measuring probe because of the boundary layer in a similar manner as at the plate surface itself. It is therefore probable that the compression in the shock takes place on an even smaller section than was measured; this can also be seen from the schlieren photograph.

An expansion occurs immediately behind the compression shock for the pressure distributions at $z = 15$, 30, and 45 millimeters. It is strongest at small distances from the wall and decreases with increasing z. Above $z \sim 75$ millimeters this expansion is no longer present. For sensitive adjustment of the schlieren knife-edge a brightening could be ascertained in the schlieren photograph at the location of the expansion. The pressure distributions were determined by means of three different measuring probes in order to ascertain a possible total pressure tube effect on these phenomena. However, all three measurements resulted in the same distribution. An explanation of this phenomenon was attempted in the last chapter.

In this case as well as for the λ-shock a continuous pressure rise can be observed within the boundary layer. It starts at x ~ 196 millimeters, that is, about 14 millimeters in front of the shock. The final pressure is reached at x ~ 260 millimeters, thus 50 millimeters behind the shock. From this there again results within the boundary layer in front of the shock a pressure gradient outwards and behind the shock a gradient inwards. (See fig. 18.) The density changes thus created are shown in the schlieren photograph (fig. 16) in the shape of a weak black line inclined outwards. The pressure rise which extends upstream beyond the compression shock within the boundary layer also causes for this case a thickening of the boundary layer. The flow deflection thus created here again leads to a small oblique compression shock located only a little ahead. (See fig. 16.) Pressure measurements in this zone were not possible because of its small extent.

B. Behaviour of the boundary layer

The boundary-layer behaviour was again determined by means of pressure measurements. Several characteristic velocity profiles are presented in figure 19.

The boundary layer in front of the compression shock is in a turbulent flow condition. Due to the expansion in front of the shock the boundary-layer profiles there become more convex. The Reynolds number, referred to the momentum thickness and the corresponding undisturbed velocity, is 1478 immediately ahead of the compression shock.

The boundary layer is thickened by the compression shock outside of it. In contrast reversed flow could not be ascertained at any point. The behaviour of the momentum thickness δ^{**} and the displacement thickness δ^{*} is plotted as a function of x in figure 20. δ^{*} increases 4.8 times from x = 140 millimeters to x = 250 millimeters, whereas δ^{**} in the same distance increases from 0.215 millimeters to 0.850 millimeters. Therefore, the boundary layer thickens for this case considerably less than for the corresponding λ-shock for which δ^{*} and δ^{**} increase approximately 10 times. This fact can also be realized from the schlieren photograph. Another notable fact for the pressure measurements in the boundary layer behind the shock was that in contrast to the λ-shock no fluctuation with time of the total pressure were noticeable.

In addition, a calculation of the shear stresses at the wall τ_0 from the boundary layer equation (9) was attempted. The values are plotted in figure 20 as functions of x. The curve shows an

increase of the shear stresses at the wall in front of the compression shock, then a decrease (due to the pressure rise) and then again a gradual increase.

C. The total pressure losses in the compression shock

The measured total pressure loss $p_o - p_p$ of the compression shock is to be seen in figure 21. Corresponding to the intensity of the compression shock the pressure losses increase with decreasing z. Within the boundary layer one finds the losses caused by friction. In the supersonic region of the boundary layer the measurement gives the sum of shock and friction losses.

Test Series IV

Characteristic data:

M = 1.1 to 1.4 variable

$Re_l \sim 2.700 \times 10^6$ constant

Boundary layer in front of the shock: turbulent

In analogy to test series II the Mach number is varied at constant Reynolds number. In contrast to the λ-shock for a laminar boundary layer no multiple compression shocks develop now even for small Mach numbers; the compression always takes place in a single stage.

Figure 22 shows the schlieren photographs for M = 1.12, 1.26, and 1.31; the pressure distributions pertaining to it at the surface of the plate are plotted in figure 23. Schlieren photographs as well as pressure distributions show a similar course for various Mach numbers.

Test Series V

Characteristic data:

Mach number of the free stream velocity constant

$Re_l = 1.3 \times 10^6$ to 2.7×10^6 variable

Boundary layer in front of the shock: for transition from laminar into turbulent.

In this test series the influence of the Reynolds number upon the compression shock was investigated. Re_l was varied continuously so that the transition from laminar to turbulent boundary layer in front of the compression shock could be observed.

The change of the Reynolds number was effected by varying the pressure and thereby the air density in the tunnel. Meanwhile the temperature in the tunnel was kept constant so that the Mach number of the free-stream velocity of the auxiliary plate remained unchanged.

The λ-shock forms the first subject of the experiments as in test series V; subsequently, the Reynolds number was increased step by step. Figure 24 contains the schlieren photographs for the following Reynolds numbers: $Re_l = 1.325 \times 10^6$, 1.570×10^6, 1.781×10^6, 2.020×10^6, 2.261×10^6, and 2.681×10^6.

The pressure measurements show that the transition from laminar to turbulent boundary layer in front of the compression shock takes place discontinuously. There are places on the plate where, due to disturbances on the surface, the turbulence appears somewhat sooner than at other points. Since the schlieren photograph represents all compressions taking place over the entire width of the tunnel one can recognize both compression shocks in a certain region of the Reynolds numbers. From the series of schlieren photographs one can clearly recognize the transition between the two types of compression shock. The oblique compression shock of the λ-shock gradually disappears for increasing Reynolds number. The part of the main shock adjoining the oblique shock towards the outside remains unchanged.

Simultaneously with the disappearance of the oblique shock which is located relatively far ahead, the main shock becomes an unbroken slightly curved line which extends to the proximity of the plate surface. At the base of this shock a small oblique compression shock still remains, as was already shown in test series II; it is clearly visible in the schlieren photographs. However, not only the influence of the change in boundary-layer condition upon the compression shock is shown but also the different behaviour of the friction layer changing its flow condition with respect to the compression shock. The decrease of the thickening of the boundary layer for increasing Reynolds number is very distinct.

A. The pressure measurements

Different pressure distributions result corresponding to the variation of the compression shocks. The two pressure distributions at the surface of the plate for the highest and lowest Reynolds number investigated are plotted in figure 25. Reliable pressure measurements were no longer possible for the intermediate steps.

B. The total pressure losses

The total pressure losses $p_o - p_p$ due to the compression shocks are plotted in figure 26. As a consequence of the higher excess velocities for the same Mach number of the free-stream velocity larger shock losses occur for the case of a turbulent boundary layer. In contrast the pressure losses in the separated and greatly thickened boundary-layer increase for the laminar condition.

Test Series VI

Characteristic data:

$M = 1.279$

$Re = 1.69 \times 10^6$

$Re_\delta{}^{**} = 1159$

With turbulence wire:

In this test the laminar boundary layer in front of the compression shock is transformed artificially into a turbulent boundary layer. The turbulence is produced by means of a wire which is stretched across the auxiliary plate at the point $x = 12$ millimeters. Diameter of the wire and distance of the wire from the surface of the plate amount to approximately 0.3 millimeter each.

The resulting compression shock can be seen in the schlieren photograph (fig. 27); it has the same character as in the case of natural turbulence. Without turbulence wire a λ-shock similar to the one in test series I occurs.

The λ-shock can therefore be avoided by artificially influencing the boundary layer. If the turbulence is to be produced by a wire, it is not necessary to place the wire at the nose of the profile, for instance. Tests have demonstrated that a turbulence wire of 0.2-millimeter thickness which is fixed on the surface shortly ahead of the main shock also fulfills the purpose. It is unfavourable to place the wire relatively far ahead of the shock in the supersonic region because then the wire itself can cause an oblique compression shock.

It is possible to produce the turbulence by still other means (for instance, by an edge or by blowing air).

A. The pressure measurements

In figure 28 the distribution of the static pressure for various distances from the wall is plotted. A pressure distribution results at the plate surface similar to that for the case of natural turbulence of the boundary layer before the shock. Outside of the boundary layer the pressure measurements result unexpectedly in two strong compressions in short succession. In agreement with the pressure measurements the schlieren photographs show two shock lines at this location. The first pressure rise in this "double shock" amounts to about 17 percent of the subsequent one, and does not lead to subsonic velocity; only after the second shock a subcritical pressure ratio is reached. A small expansion takes place between the two compression shocks as can be seen from pressure measurement and schlieren photograph. Both measuring methods (as in test series III) give a post-expansion following the second compression. Here also this post-expansion falls off with increasing distance from the wall and is no longer present outside of $z = 80$ millimeters.

Two such compression shocks in short succession were also observed for the case of natural turbulence of the boundary layer. (See fig. 22.) For certain conditions it is also possible that the first small shock extends only over a fraction of the total shock extent in z-direction. (See test series VII.) It starts, however, in all cases observed in the supersonic region of the friction layer.

Presumably this "double shock" represents a condensation phenomenon. It was possible to calculate from humidity measurements that for the pressure ratio $p/p_0 = 0.52$ approximately the saturation condition (ice formation) [sic] is reached. At any rate it does not seem possible to explain the first (almost) normal shock which leads from supersonic to supersonic by means of the ordinary shock equations.

B. The behaviour of the boundary layer

From the measurements there results a behaviour of the boundary layer similar to the one in test series III (natural turbulence). Several characteristic velocity profiles are represented in figure 29. In figure 30 the behaviour of δ^* and δ^{**} as functions of x can be seen.

The boundary layer can overcome the pressure rise without the occurrence of reversed flow. As in the case of natural turbulence, also here a small oblique compression shock near the wall appears which meets the main shock at a distance from the wall of approximately 10 millimeters.

C. The shock loss

The shock loss $p_o - p_p$ in the compression shock is plotted in figure 31. Its behaviour as well as the absolute values are similar to those of test series III.

Test Series VII

Characteristic data:

$M = 1.306$

$Re_\delta{}^{**} = 2315$

Boundary layer: turbulent

The test was carried out without auxiliary plate, that is, on the lower nozzle wall. On this wall there is a thick turbulent boundary layer. $Re_\delta{}^{**}$ ahead of the shock is 2315; it was $Re_\delta{}^{**} = 1479$ in the case of the turbulent boundary layer on the auxiliary plate. The schlieren photographs of the compression shock can be seen from figure 32.

A. The pressure measurements

The distribution of the static pressure at various distances from the wall is plotted in figure 33.

For this pressure again a weaker pressure gradient than in undisturbed flow results at the wall. Outside of the boundary layer the compression takes place up to a distance from the wall of $z \sim 75$ millimeters by means of two shocks in short succession.

The compression in the first shock is essentially smaller than the one of the second shock. Between the two compression shocks a slight expansion takes place. This behaviour is similar to the behaviour ascertained in test series VI (turbulence wire), with the difference, however, that now outside of a certain distance from the wall the compression takes place in a single shock.

Pressure measurements and schlieren photographs show good agreement here also. Another weak compression line is present in the schlieren photographs ahead of the shock which is an effect of the side walls.

Behind the compression shock an expansion which decreases with increasing distance from the wall takes place as in other tests.

B. The behaviour of the boundary layer

Several characteristic boundary-layer profiles are plotted in figure 34. The course of δ^* and δ^{**} can be seen from figure 35. Reversed flow of the boundary layer does not occur at any point. Due to the pressure rise the boundary layer is thickened; separation does not occur.

C. The pressure loss in the shock

The pressure loss caused by the compression shock was measured at the point $x = 70$ millimeters as a function of the distance from the wall. (See fig. 36.) The distribution is similar to the one in the other test series for turbulent boundary layer ahead of the shock.

SUMMARY OF THE EXPERIMENTAL RESULTS

1. The flow phenomena depend essentially on whether or not the flow of the boundary layer ahead of the shock is laminar or turbulent.

2. For laminar boundary layer and for Mach numbers not far exceeding 1, multiple shocks occur which decrease in number when the velocity is increased. Finally a simple λ-shock is reached.

3. The λ-shock consists essentially of a normal main shock with a preceding oblique compression shock. In front of the main shock the flow of the boundary layer is still laminar; the reversed

flow in the proximity of the wall causes a large increase of the displacement thickness in the direction of the flow which is found to be in good agreement with the deflection of the supersonic flow by the oblique shock. Behind the main shock the boundary layer is turbulent.

4. Turbulent boundary layers give only normal shocks, independent of the Reynolds and Mach numbers. It does not matter whether the boundary layer becomes turbulent naturally (for instance by increase of the Reynolds number) or artificially (with disturbance wire).

5. The displacement thickness of the boundary layer increases considerably on going through the shock, more so for laminar than for turbulent layers.

6. Behind the main shock the pressure falls off rapidly at some places. It seems that this fact is by no means due to errors in measurement but that this falling off can be explained from the behavior of frictionless gas flows by quick pressure adjustments of differences in the flow intensity just under sonic velocity. (Compare the following note.)

7. Formations of normal double shocks close to each other have been observed in the schlieren photograph and it was determined by means of pressure measurements that this phenomenon really occurs in the flow. It can probably be connected with ice precipitation.

8. Compared with the strong pressure rise in the shock outside of the boundary layer the pressure rise at the wall takes place much more gradually. In connection with it pressure gradients perpendicular to the wall originate in the region where the shock borders on the wall; these gradients are also visible in the schlieren photograph.

REMARKS CONCERNING THE FALLING OFF OF PRESSURE BEHIND THE MAIN SHOCK

For the pressure distribution at the distance from the wall $z = 15$, 30, and 45 millimeters (fig. 17) a strong expansion was observed immediately behind the compression shock. These pressure distributions were plotted separatively in figure 37; the theoretical final pressures behind the shock resulting from the condition before

the shock according to the shock equations were also plotted. The calculated values show good agreement with the measured pressure behind the shock, that is, in front of the subsequent expansion.

The "post-expansion" decreases with increasing distance from the wall. For $z = 60$ millimeters and $z = 75$ millimeters the theoretical final pressure behind the shock is even smaller than the one that was observed. (See fig. 37.) This fact suggests that a "post-compression" takes place here which is very strong, like the post-expansion, so that it has a steepness of a similar order of magnitude as that of the shock itself.

One obtains a qualitative explanation of this phenomenon if one takes Prandtl's relation

$$w_1 w_2 = a^{*2} \tag{15}$$

into consideration. w_1 and w_2, respectively, are the velocities in front of and behind the normal shock; a^* is the critical sonic velocity which depends only on the stagnation temperature and is therefore constant in the entire flow field. From (15) follows that the greater the supersonic velocity in front of the shock, the smaller becomes the subsonic velocity behind the shock.

For the present tests a limited supersonic region was produced by slight curvature of the plate. Along a line perpendicular to the plate the supersonic velocity will decrease more and more with increasing distance from the wall; apart from the boundary layer one finds the highest velocity in the immediate proximity of the wall. If now a normal shock exists in this supersonic region, there results according to Prandtl's equation (15) the smallest subsonic velocity in the proximity of the wall; the velocity behind the shock will increase with the distance from the wall. Such a velocity distribution, however, will certainly be changed by the boundary conditions which the curved plate imposes on the flow: near the wall a post-acceleration (that is, post-expansion) will take place; on the other hand at a larger distance from the wall a post-deceleration (that is, post-compression) must result.

The striking steepness of these pressure distributions is at least partly explained by the compressibility of the flow. It seems that disturbances in the longitudinal velocity as they exist here die off much faster in the compressible than in an incompressible flow. As a simple example the potential flow for parallel motion with a small periodic disturbance of the velocity (and

therefore also of the pressure) is investigated. At a point $x = 0$ let the dependence of the longitudinal velocity w_x on the distance from the wall z (fig. 38) be:

$$w_x = w_o + \Delta w \cos \frac{2\pi z}{t} \tag{16}$$

Δw is the "amplitude," t the "wave length" of the disturbance.

Similar to the procedure in the investigation of a slightly wavy wall with parallel flow the flow is first regarded as incompressible and compressibility taken into account afterwards by application of Prandtl's rule. For the incompressible case the condition of the imposed velocity distribution is fulfilled by the potential

$$\Phi = w_o x - \frac{\Delta w t}{2\pi} \cos \frac{2\pi z}{t} e^{-\frac{2\pi x}{t}} \tag{17}$$

from which follows:

$$w_x = w_o + \Delta w \cos \frac{2\pi z}{t} e^{-\frac{2\pi x}{t}} \tag{17(a)}$$

$$w_z = \Delta w \sin \frac{2\pi z}{t} e^{-\frac{2\pi x}{t}} \tag{17(b)}$$

If one seeks the corresponding Φ as a solution of the linearized potential equation for compressible flow, that is, of the equation

$$(1 - M^2)\frac{\partial^2 \Phi}{\partial x^2} + \frac{\partial^2 \Phi}{\partial z^2} = 0$$

with $M = w_o/a$, one can see from the form

$$\frac{\partial^2\Phi}{\partial x^2} + \frac{\partial^2\Phi}{\partial(z\sqrt{1 - M^2})^2} = 0$$

that in the incompressible potential (17) z must be replaced by $z\sqrt{1 - M^2}$

$$\Phi = w_o x - \frac{\Delta w t}{2\pi} \cos \frac{2\pi z\sqrt{1 - M^2}}{t} e^{-\frac{2\pi x}{t}} \tag{18}$$

$$w_x = w_o + \Delta w \cos \frac{2\pi z\sqrt{1 - M^2}}{t} e^{-\frac{2\pi x}{t}} \tag{18(a)}$$

$$w_z = \sqrt{1 - M^2}\, \Delta w \sin \frac{2\pi z\sqrt{1 - M^2}}{t} e^{-\frac{2\pi x}{t}} \tag{18(b)}$$

For $x = 0$ one obtains from (18(a)) the superimposed velocity distribution with the same amplitude but with changed wave length. Therefore, one equates $t/\sqrt{1 - M^2} = t^*$; therewith w_x and w_z become

$$w_x = w_o + \Delta w \cos \frac{2\pi z}{t^*} e^{-\frac{2\pi x}{t^*\sqrt{1-M^2}}} \tag{19(a)}$$

$$w_z = \sqrt{1 - M^2}\, \Delta w \cos \frac{2\pi z}{t^*} e^{-\frac{2\pi x}{t^*\sqrt{1-M^2}}} \tag{19(b)}$$

A comparison of the velocities (17) and (19) shows that the disturbances of the parallel flow fall off very rapidly downstream when the Mach number approaches 1.

It was assumed that the disturbances can be derived from a potential, that is, that an excess in pressure corresponds to a lack of velocity and vice versa. This assumption will not be exactly fulfilled behind a shock due to the shock losses, that is, because of the deviation from the adiabatic change in state in the shock. For the present weak shocks, however, this deviation is for these considerations negligible.

Quantitatively the rule is that, for parallel flow, the longitudinal disturbances fall off $1/\sqrt{1 - M^2}$ times steeper than for the incompressible case. For the complicated flow phenomenon behind the shock the assumed flow is certainly too simplified to permit quantitative conclusions to be drawn from it, even though the results point in the direction of the observed results. (See fig. 39.)

Translated by Mary L. Mahler
National Advisory Committee
for Aeronautics

APPENDIX

LIST OF SOME FORMULAS AND CURVES FOR THE NORMAL COMPRESSION SHOCK

$$w_1 w_2 = a^{*2} = \frac{p_2 - p_1}{\rho_2 - \rho_1} = \frac{\Delta p}{\Delta \rho}$$

$$M_1^* M_2^* = 1$$

$$\frac{p_{o_2}}{p_{o_1}} = M_1^{*2} \left(\frac{1 - \frac{k-1}{k+1} M_1^{*2}}{1 - \frac{k-1}{k+1} M_2^{*2}} \right)^{\frac{1}{k-1}}$$

$$\frac{\Delta p}{p_1} = \frac{2k}{k+1} (M_1^2 - 1)$$

$$\frac{\Delta \rho}{\rho_1} = M_1^{*2} - 1$$

$$\left(1 - \frac{T_1}{T_o}\right)\left(1 - \frac{T_2}{T_o}\right) = \left(\frac{k-1}{k+1}\right)^2$$

Generally

$$M^2 = \frac{2M^{*2}}{(k + 1) - (k - 1)M^{*2}}$$

Subscript 1 or 2 designate the value in front of or behind the shock. The adiabatic stagnation pressures in front of the shock (p_{o1}) and behind the shock (p_{o2}) are not equal: the pitot pressures, however, are equal since a shock develops in the supersonic region ahead of the pitot tube. (See fig. 40.)

Therefore: $p_p = p_{p1} = p_{p2} = p_{o2}$

Figure 41 contains several curves which can be used for the investigation of normal shocks.

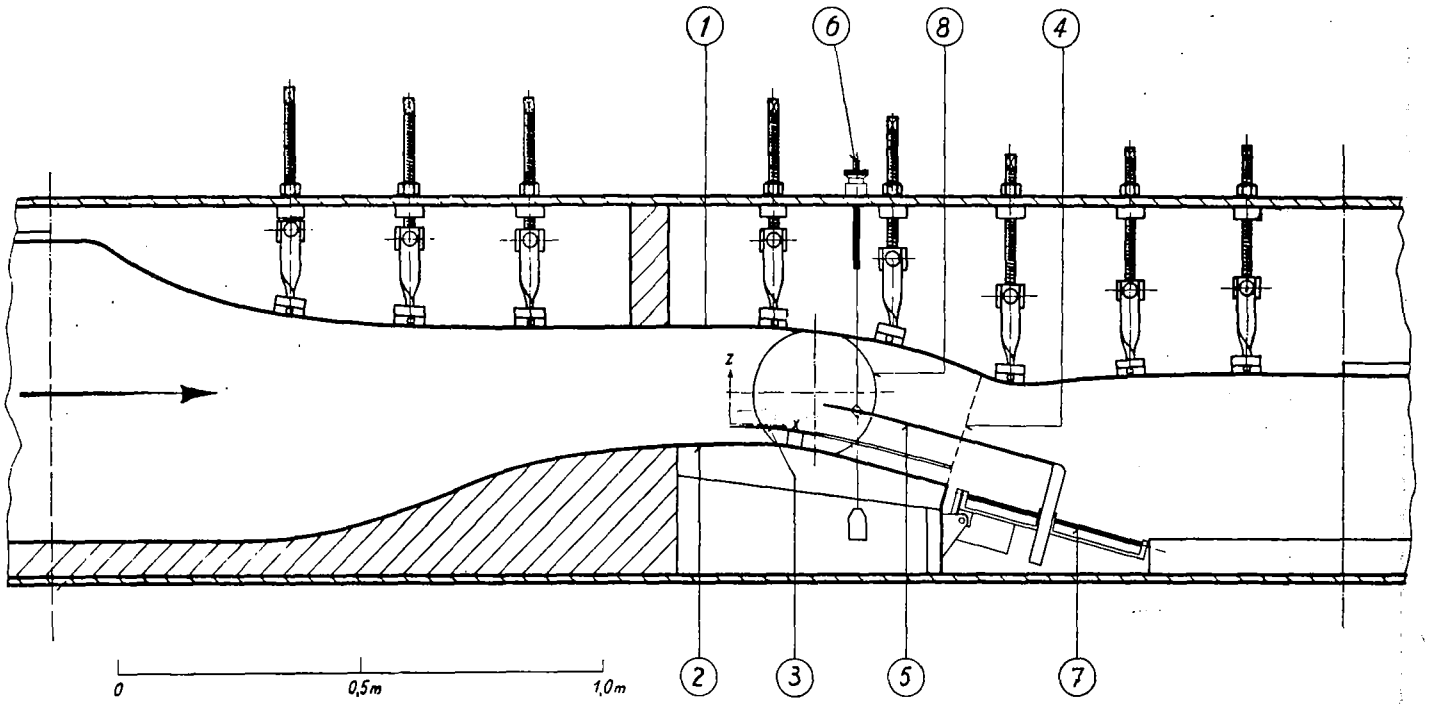

Figure 1.- Test section. 1. Upper wall of nozzle. 2. Lower wall of nozzle. 3. Auxiliary plate. 4. Minimum cross section. 5. Total pressure tube or static pressure probe. 6. Mechanism for adjusting total pressure tube in the z - direction. 7. Mechanism for adjusting total pressure tube in the x - direction.

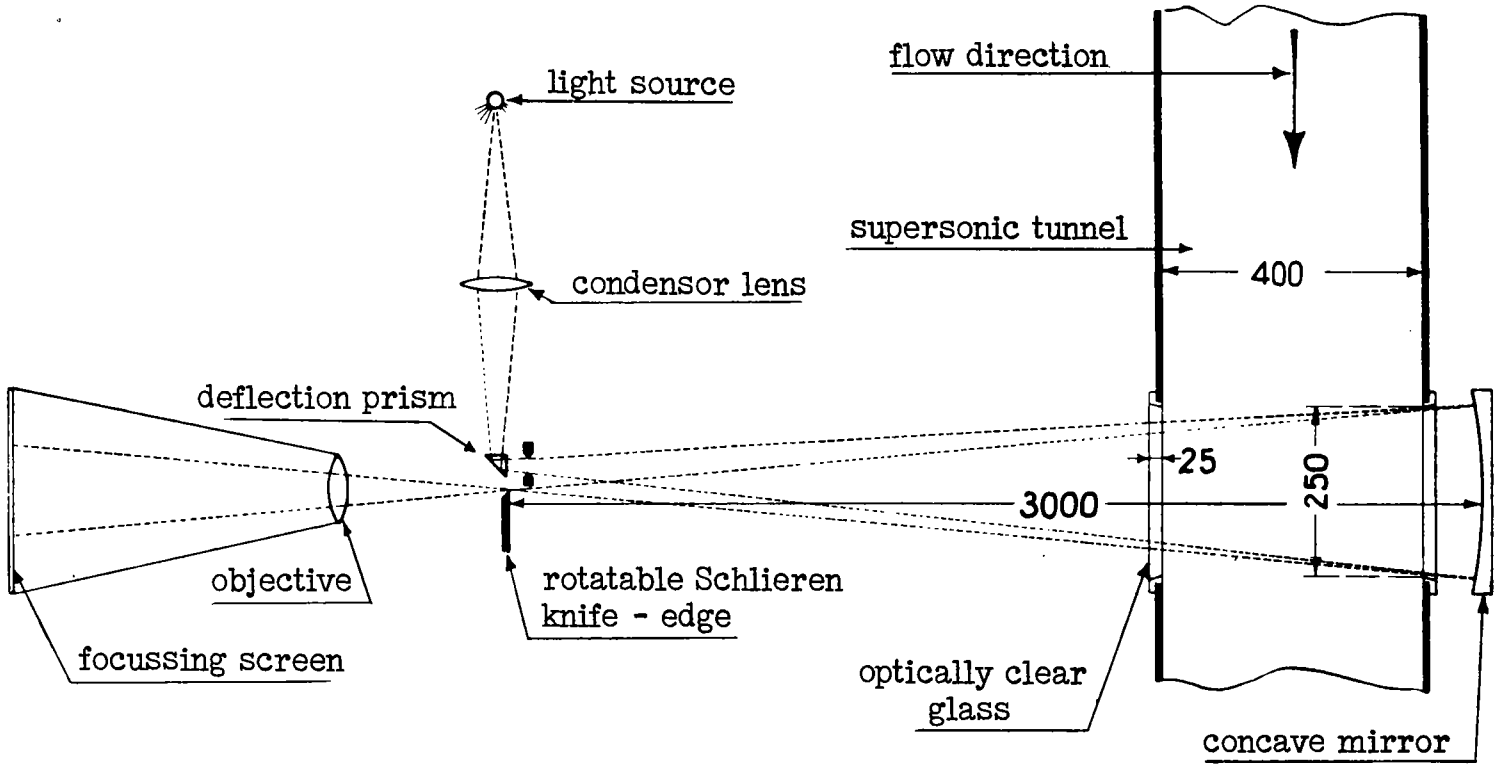

Figure 2.- Path of rays of the Schlieren optical system in schematic representation.

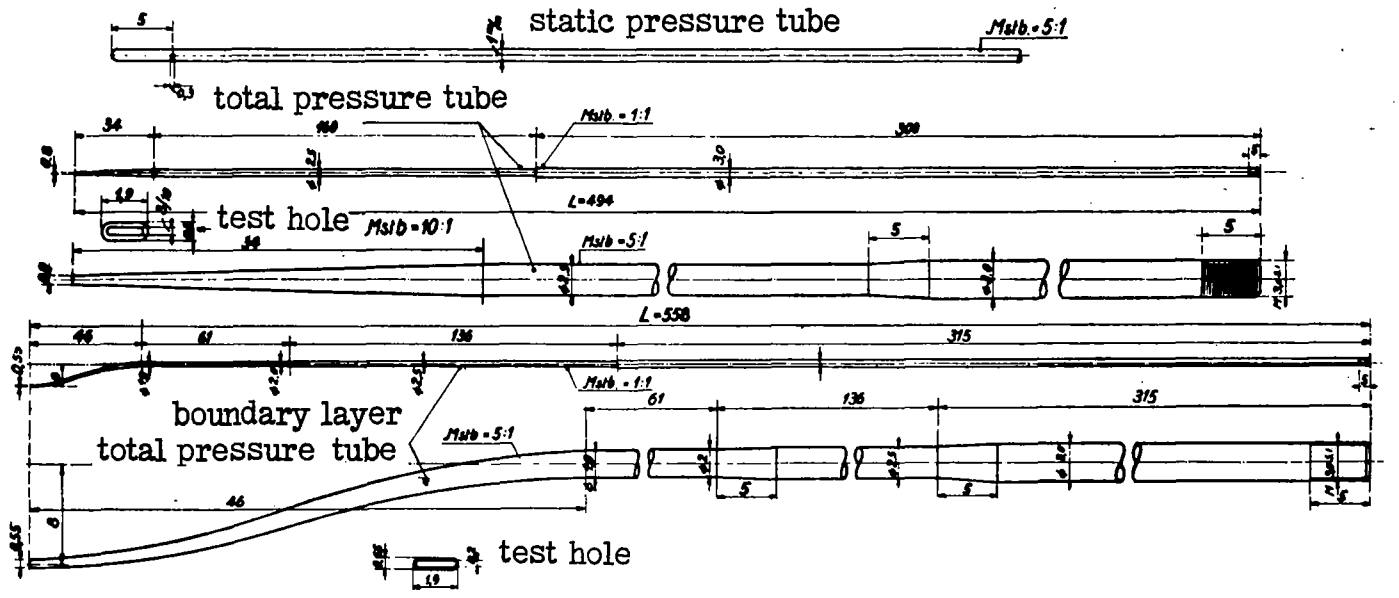

Figure 3.- Total pressure tubes and static pressure probe for measurement of static pressure.

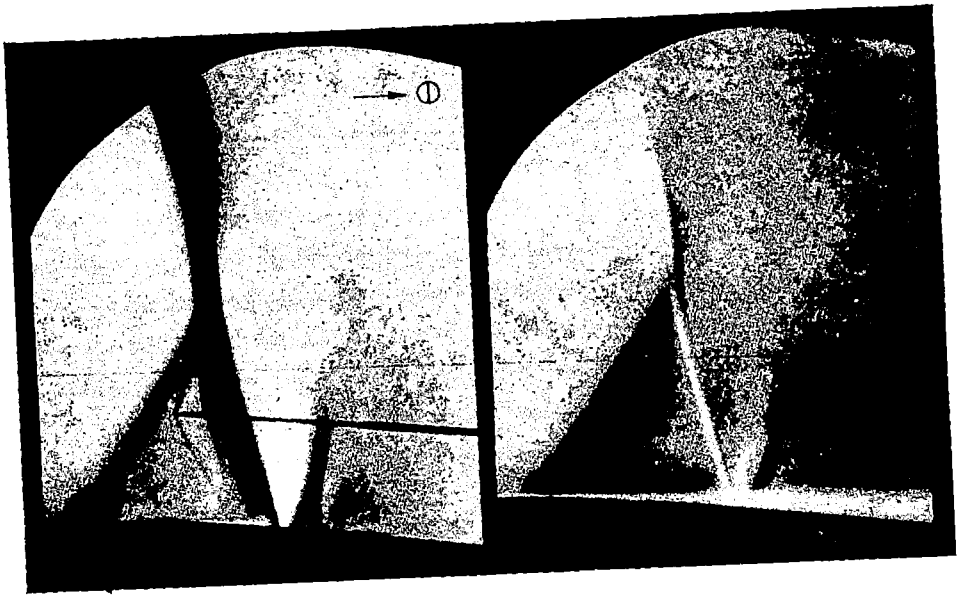

Figure 4.- Schlieren photograph λ-shock, compression shock for laminar boundary layer. $M = 1.225$, $Re_l = 1.325 \times 10^6$, $Re_\delta{}^{**} = 440$.

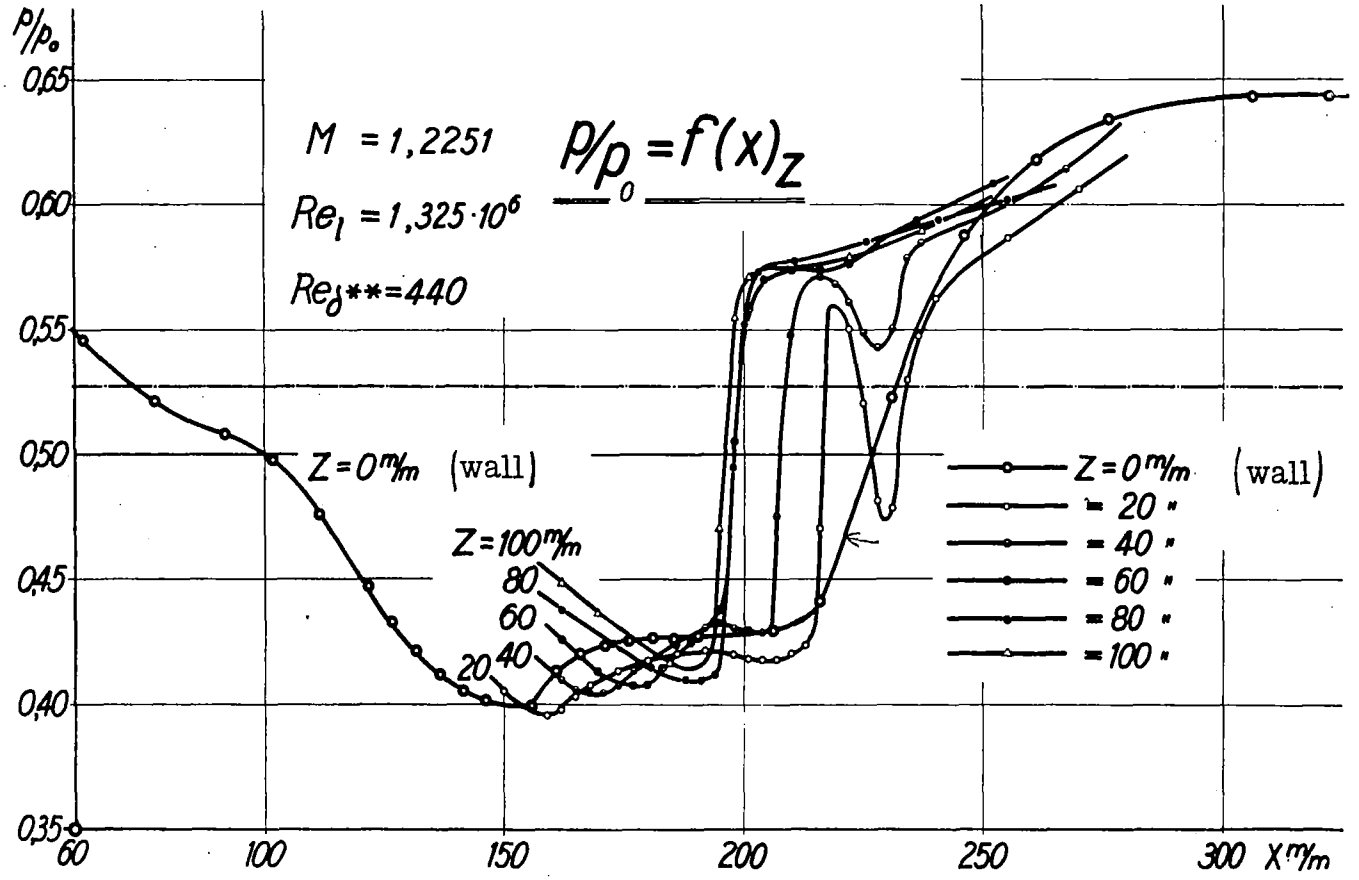

Figure 5.- λ-shock. Distribution of the static pressure at various distances from the wall. $p/p_o = f(x)_z$.

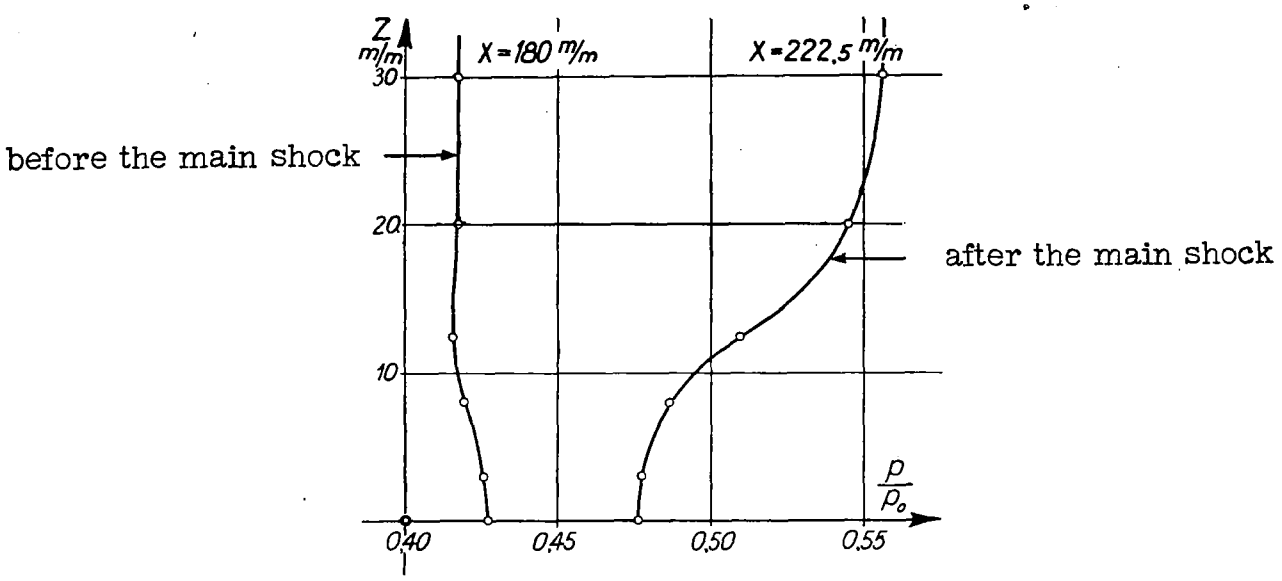

Figure 6.- λ-shock. Distribution of the static pressure as a function of the distance from the wall.

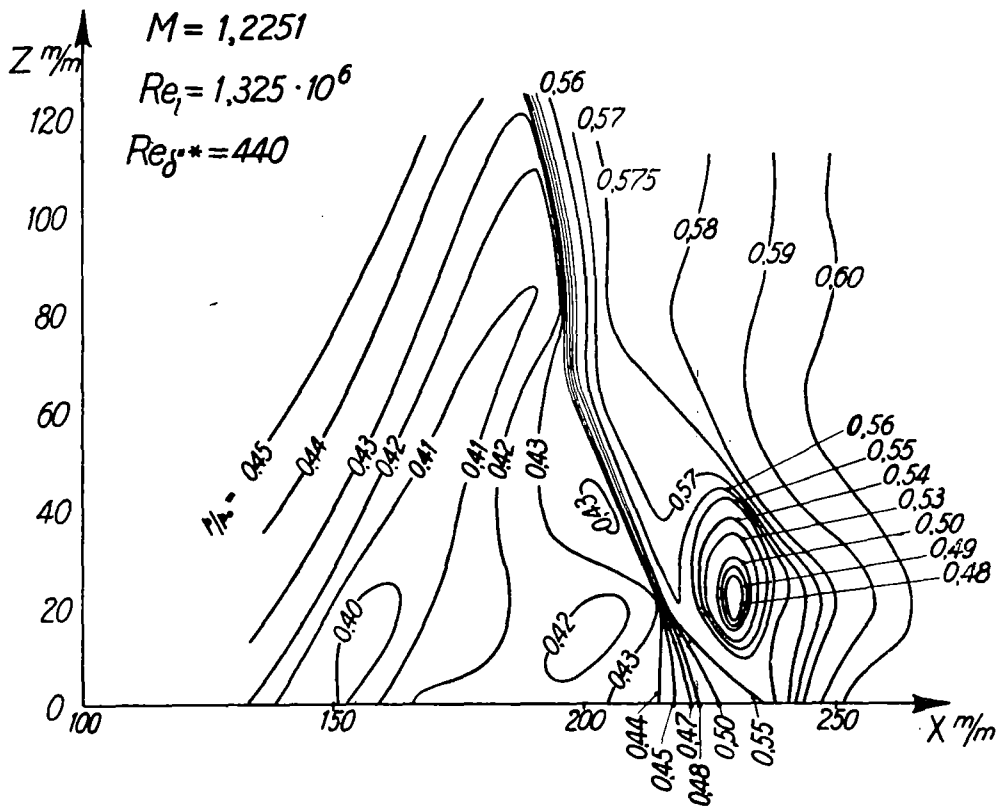

Figure 7.- λ-shock. Isobars.

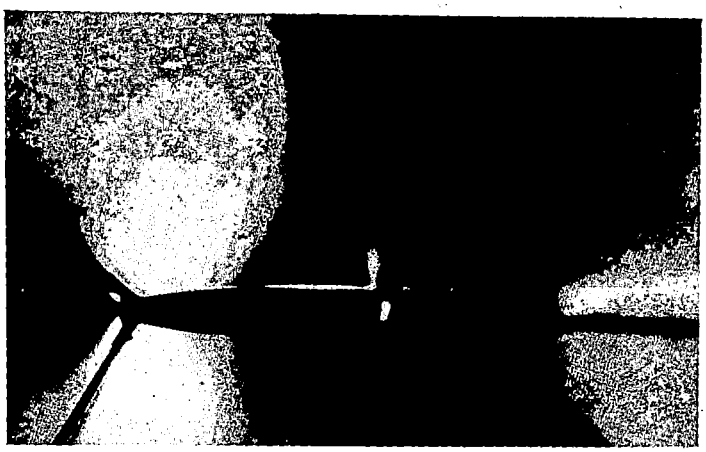

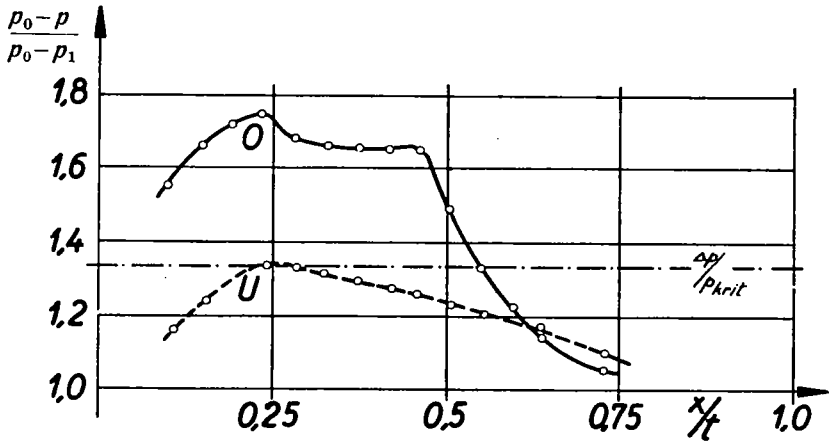

Figure 8.- Schlieren photograph and pressure distribution on a wing profile. M(of the free stream velocity) = 0.82. d/t = 10%, α = 2.6°, c_a = 0.268, $Re_t \sim 350000$.

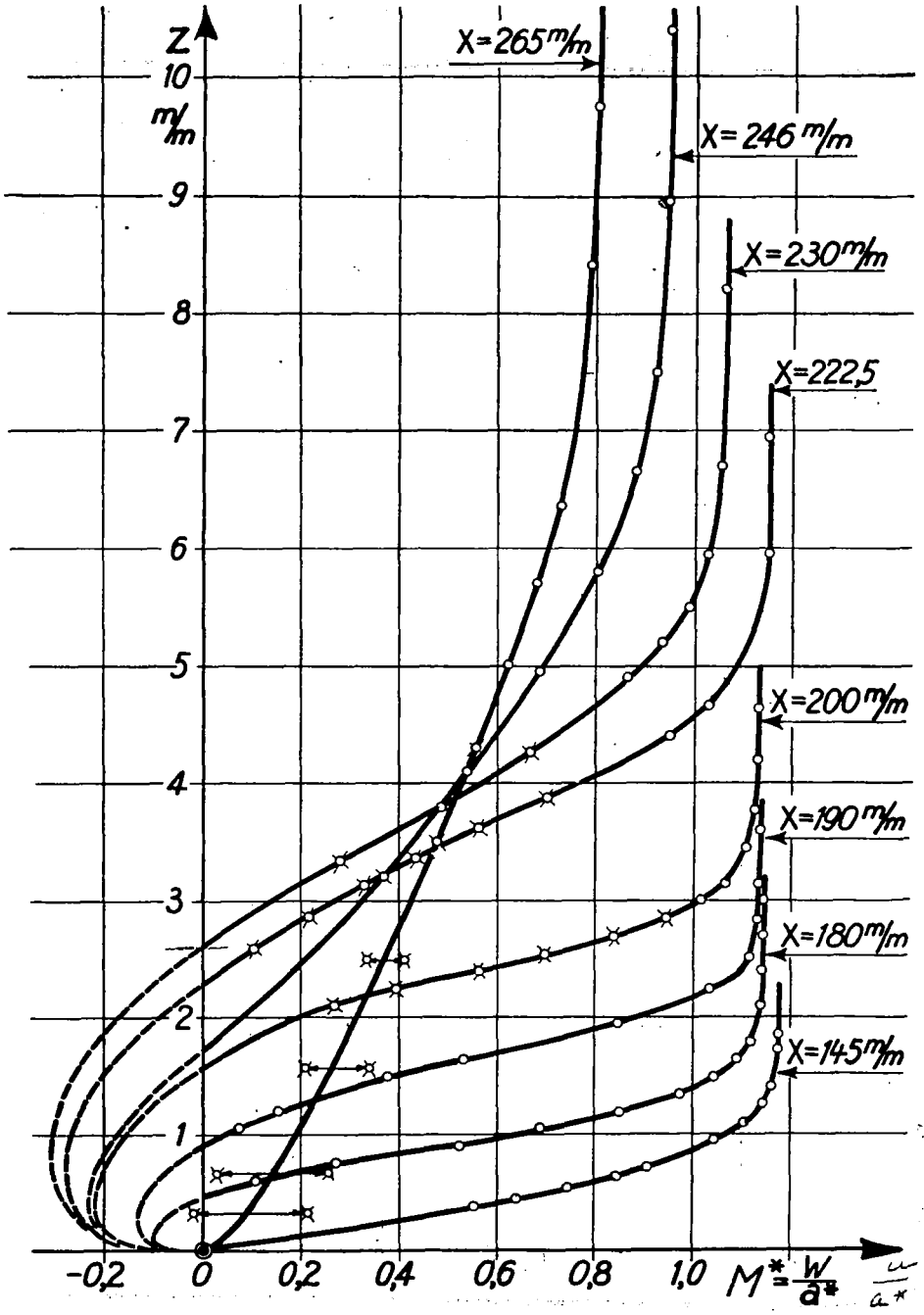

Figure 9.- λ-shock. Boundary layer profiles. $M^* = \frac{W_*}{a} = f(z)_x$.
Fluctuations in pressure are indicated by dots with cross, regions of fluctuations by arrows.

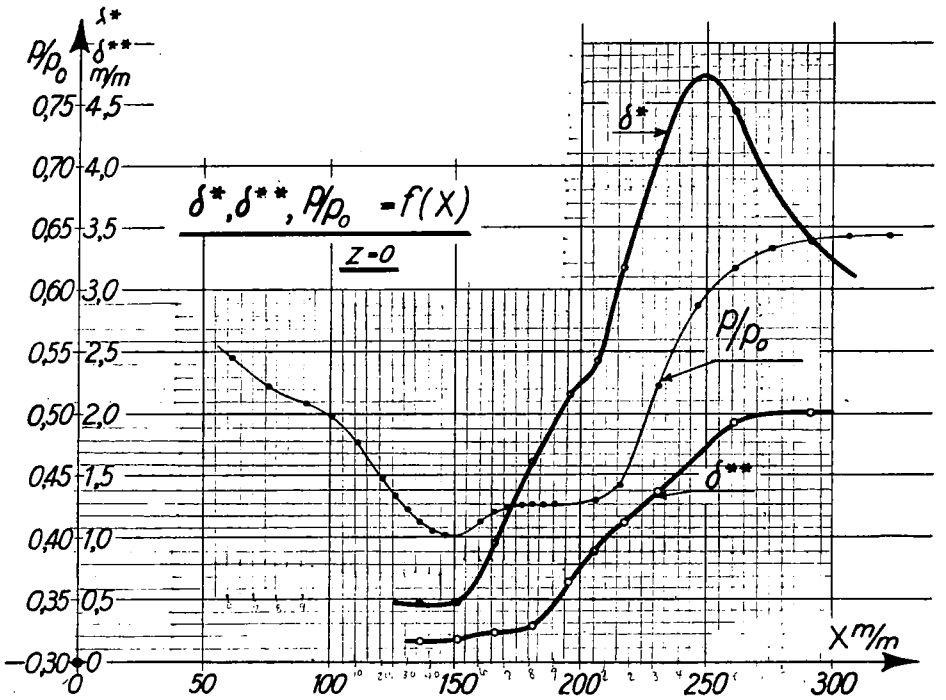

Figure 10.- λ-shock. Distribution of the displacement thickness δ* and the momentum thickness δ** of the boundary layer.

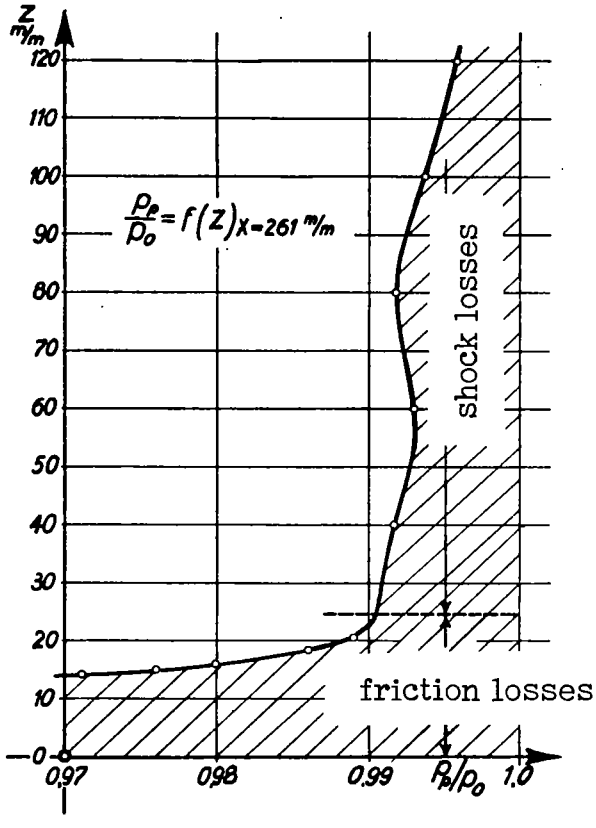

Figure 11.- λ-shock. Total pressure loss in the compression shock.

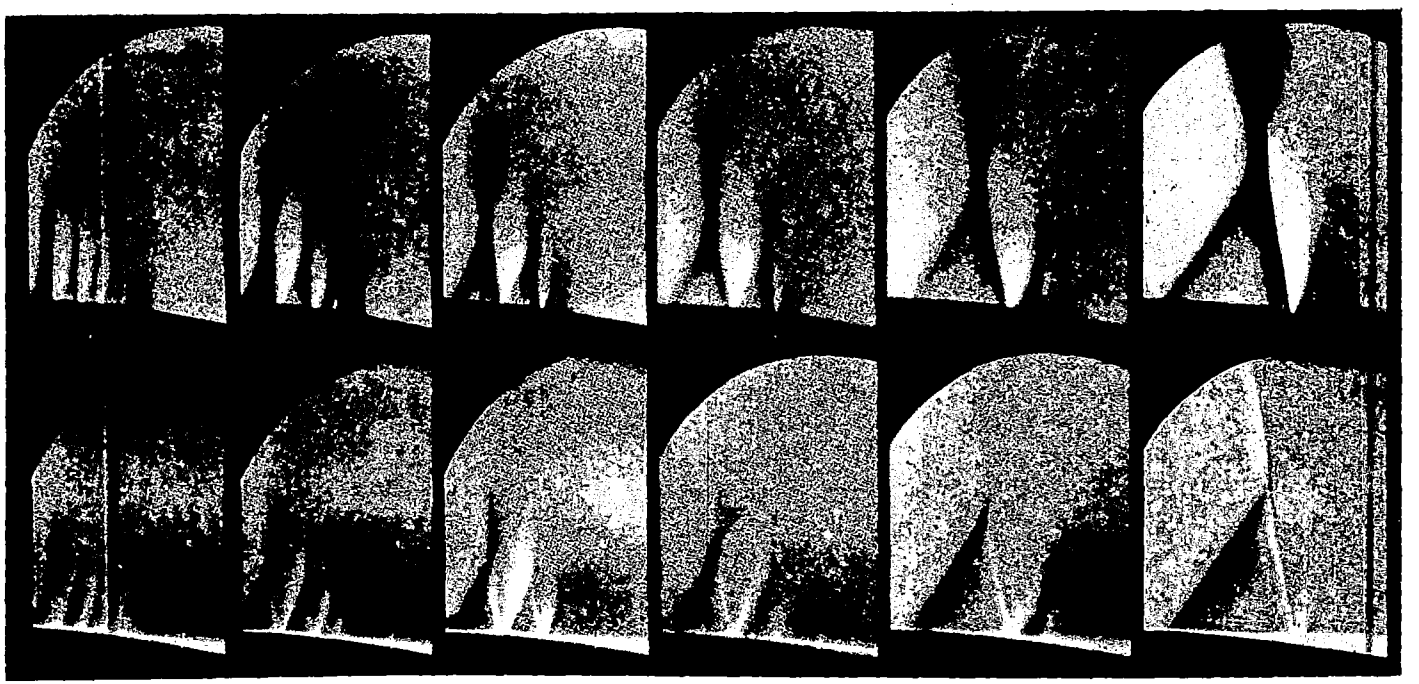

M=1.106 1.141 1.195 1.204 1.223 1.303

Figure 12.- Schlieren photographs. Laminar boundary layer in front of the shock. Variation of the Mach number for constant Reynolds number; $Re_l \sim 1.325 \times 10^6$.

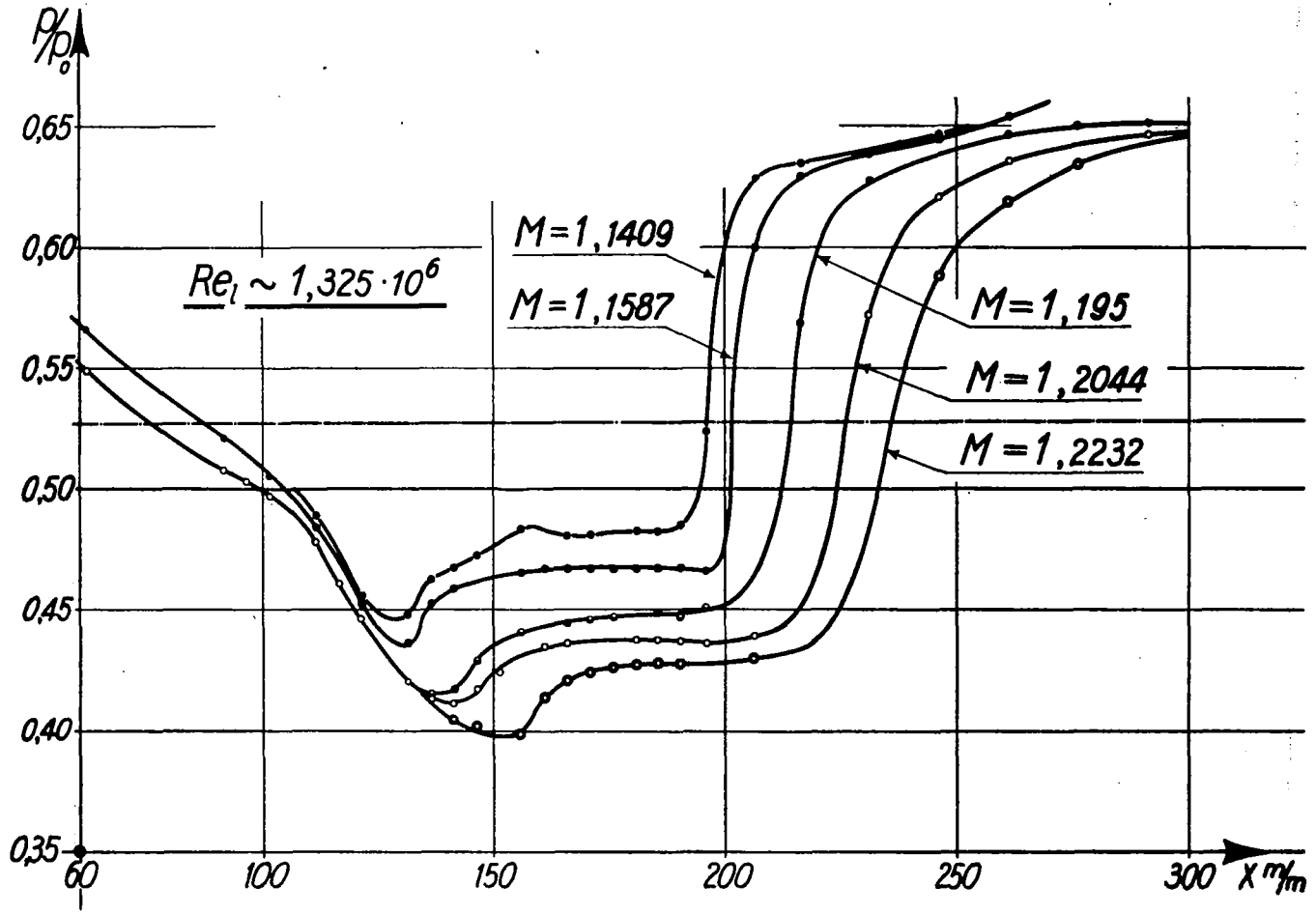

Figure 13.- Pressure distribution at the plate surface for λ-shocks for various Mach numbers. $Re_{\widetilde{l}}$ 1.325 [sic] = constant.

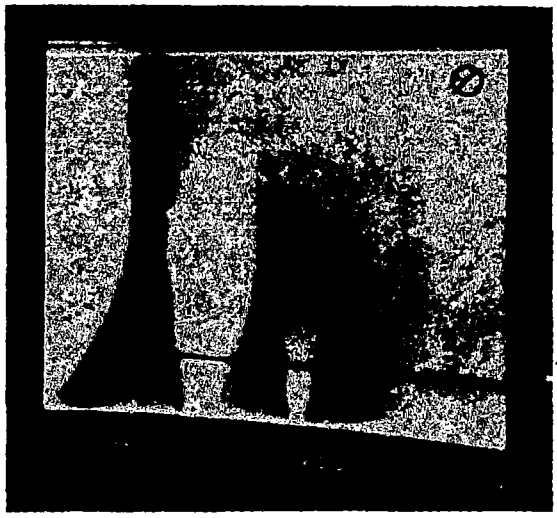

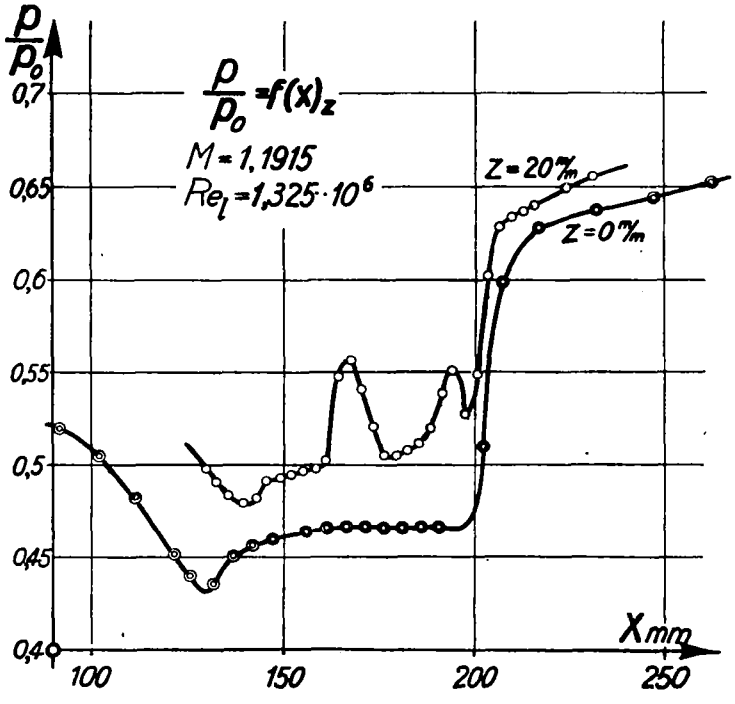

Figure 14.- λ-shock. M = 1.191. Schlieren photograph and distribution of the static pressure at the plate surface and at 20 mm distance from the plate.

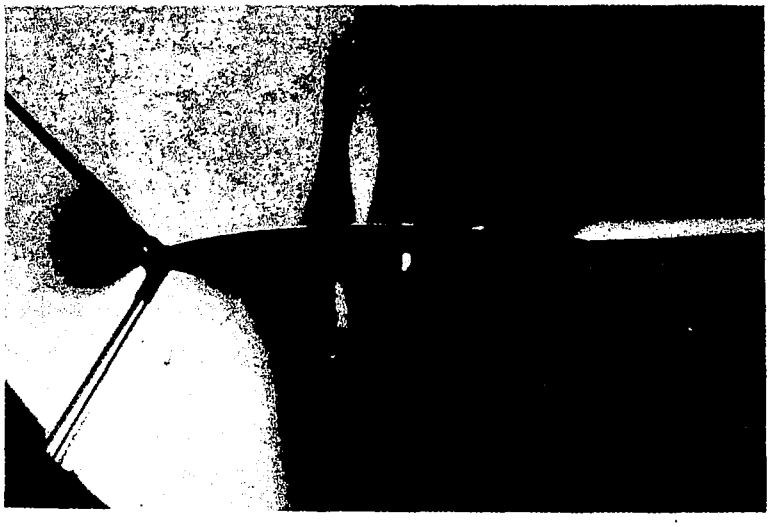

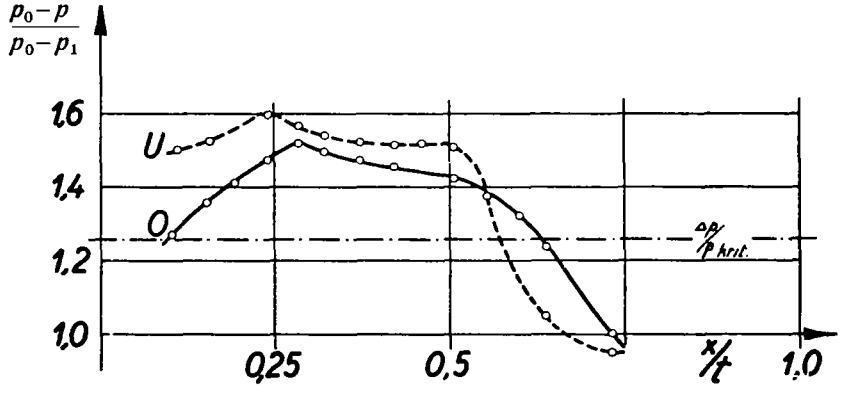

Figure 15.- Schlieren photograph and pressure distribution on a wing profile. M(of the free stream velocity) = 0.845. d/t = 10%, α = -1.6°, c_a = 0.067, Re_t = 350000.

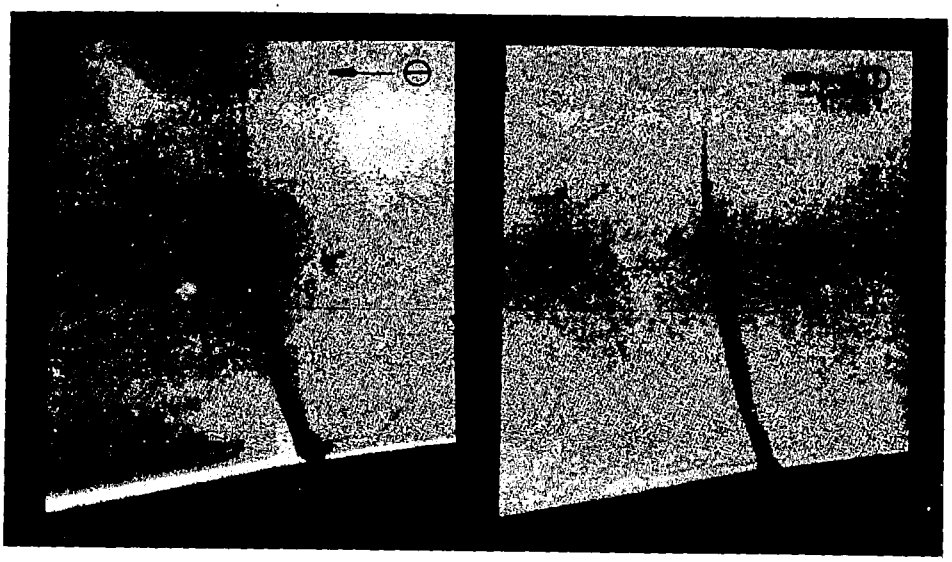

Figure 16.- Schlieren photograph. Compression shock for turbulent boundary layer. $M = 1.322$, $Re_l = 2.63 \times 10^6$, $Re_{\delta^{**}} = 1478$.

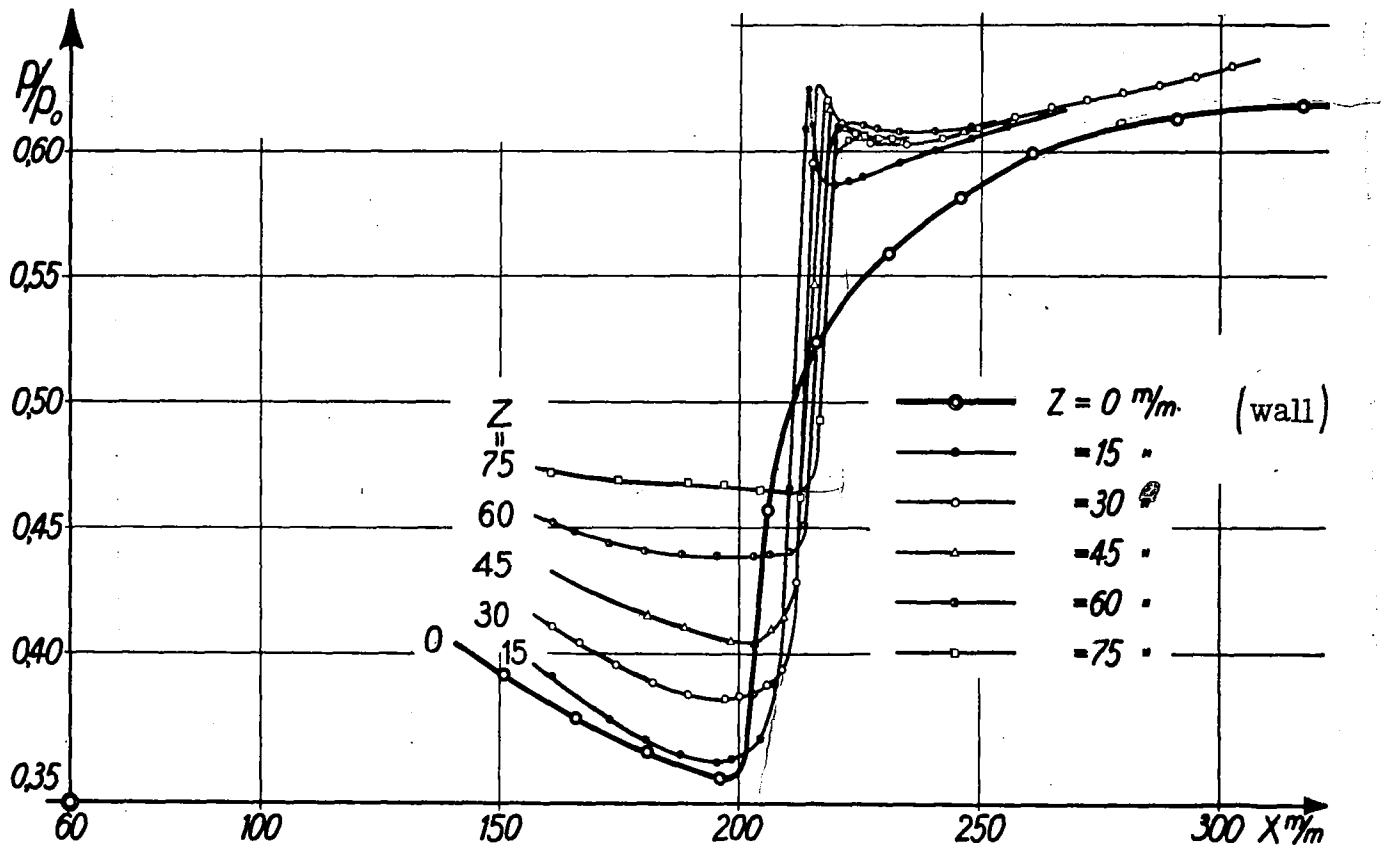

Figure 17.- Turbulent boundary layer in front of the compression shock. Pressure distribution at various distances from the wall: $p/p_o = f(x)_z$. $M = 1.322$, $Re_l = 2.63 \times 10^6$.

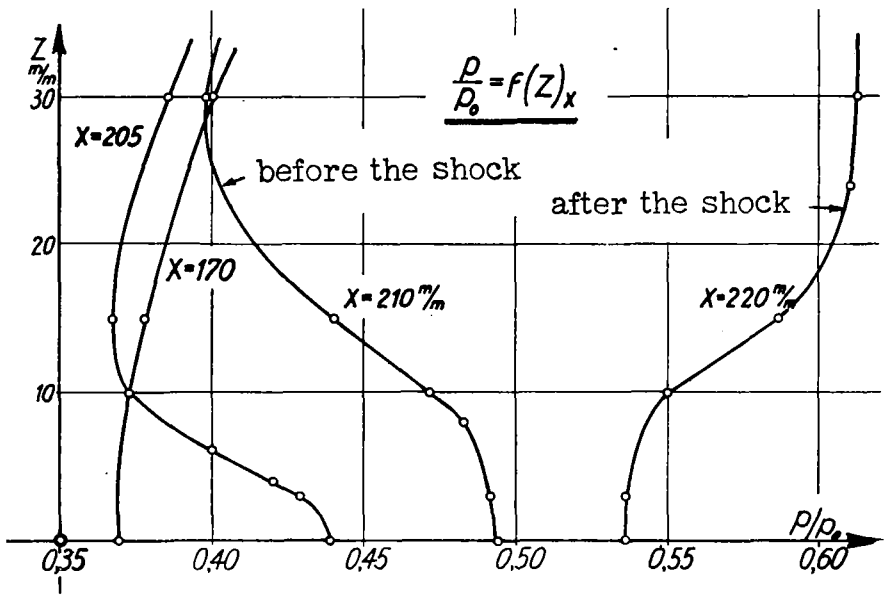

Figure 18.- Distribution of the static pressure as a function of the distance from the wall z.

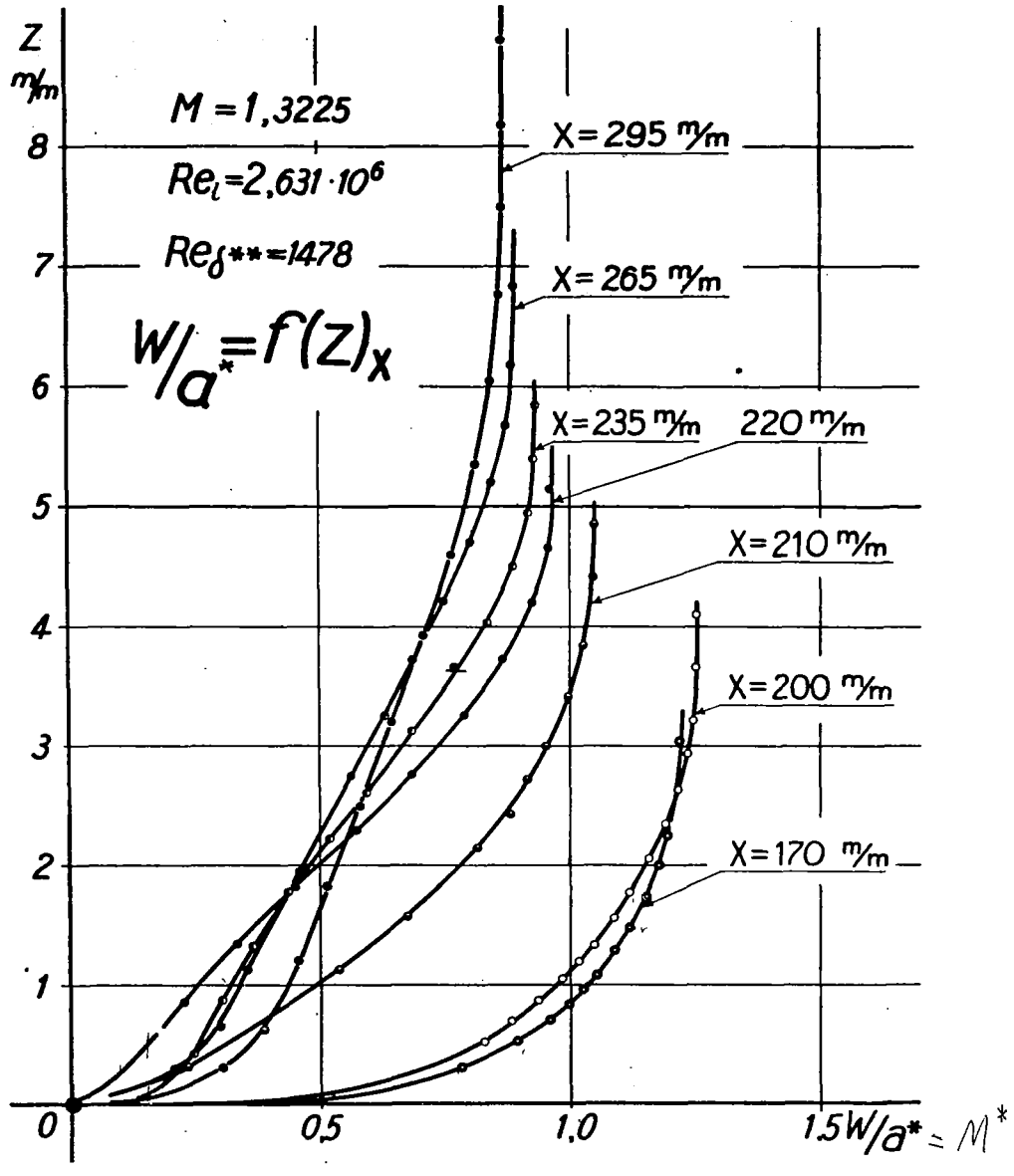

Figure 19.- Boundary layer profiles. $M^* = f(z)_x$, $M = 1.3225$, $Re_l = 2.63 \times 10^6$, $Re_\delta^{**} = 1478$. (Turbulent boundary layer in front of the shock).

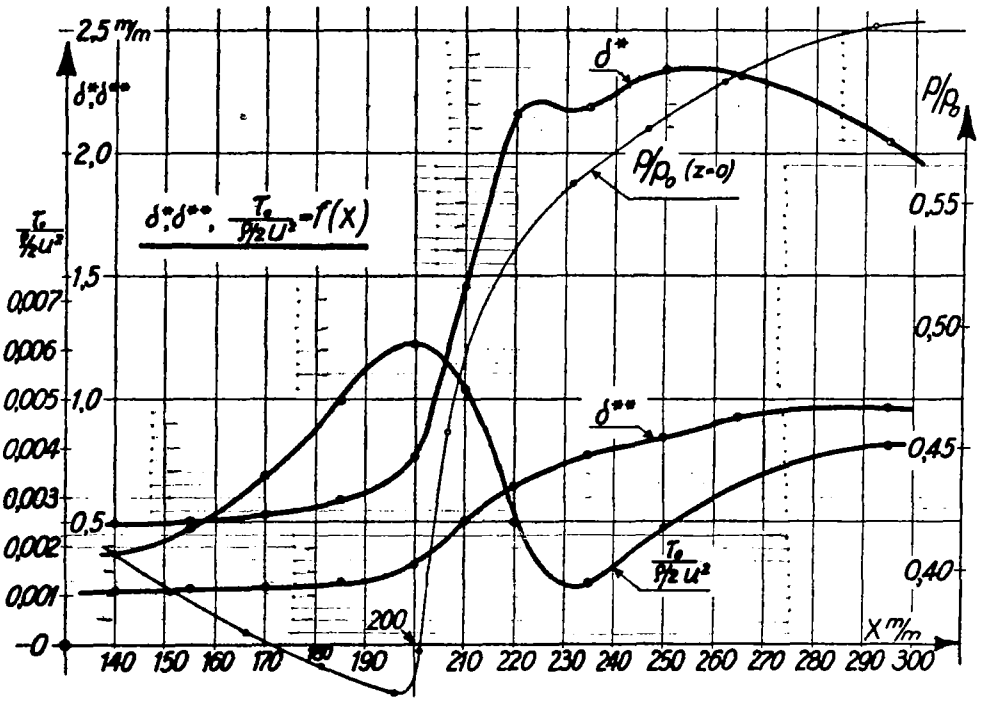

Figure 20.- Distribution of the displacement thickness δ^*, the momentum thickness δ^{**} and the shear stresses at the wall τ_o. M = 1.322, $Re_l = 2.63 \times 10^6$, $Re_{\delta^{**}} = 1478$.

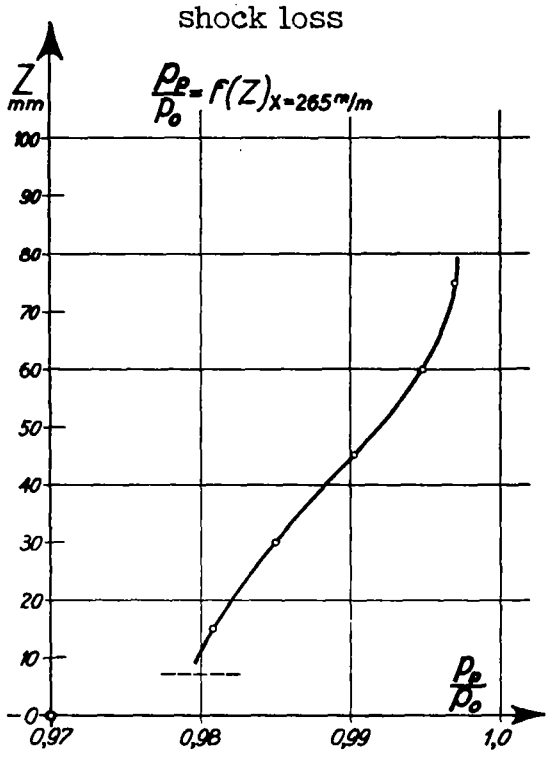

Figure 21.- M = 1.322, $Re_l = 2.63 \times 10^6$, $Re_\delta{}^{**} = 1478$. Total pressure loss in the compression shock.

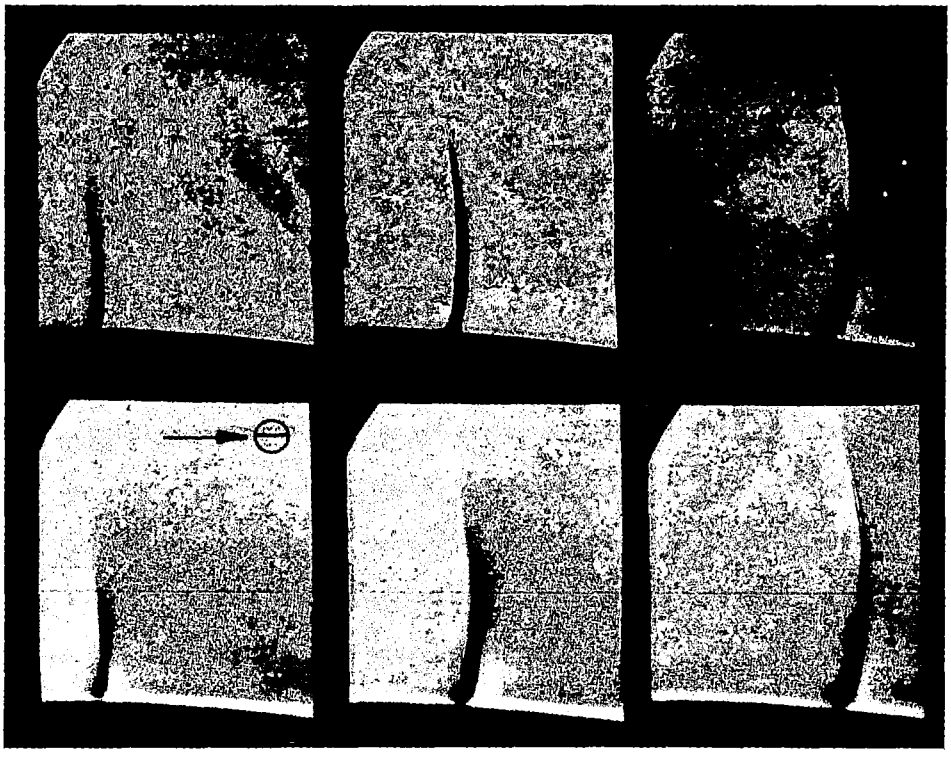

M = 1.12 1.26 1.31

Figure 22.- Schlieren photograph. Influence of the Mach number on the compression shock for turbulent boundary layer. $Re_{\tilde{l}} \sim 2.7 \times 6 \sim$ constant.

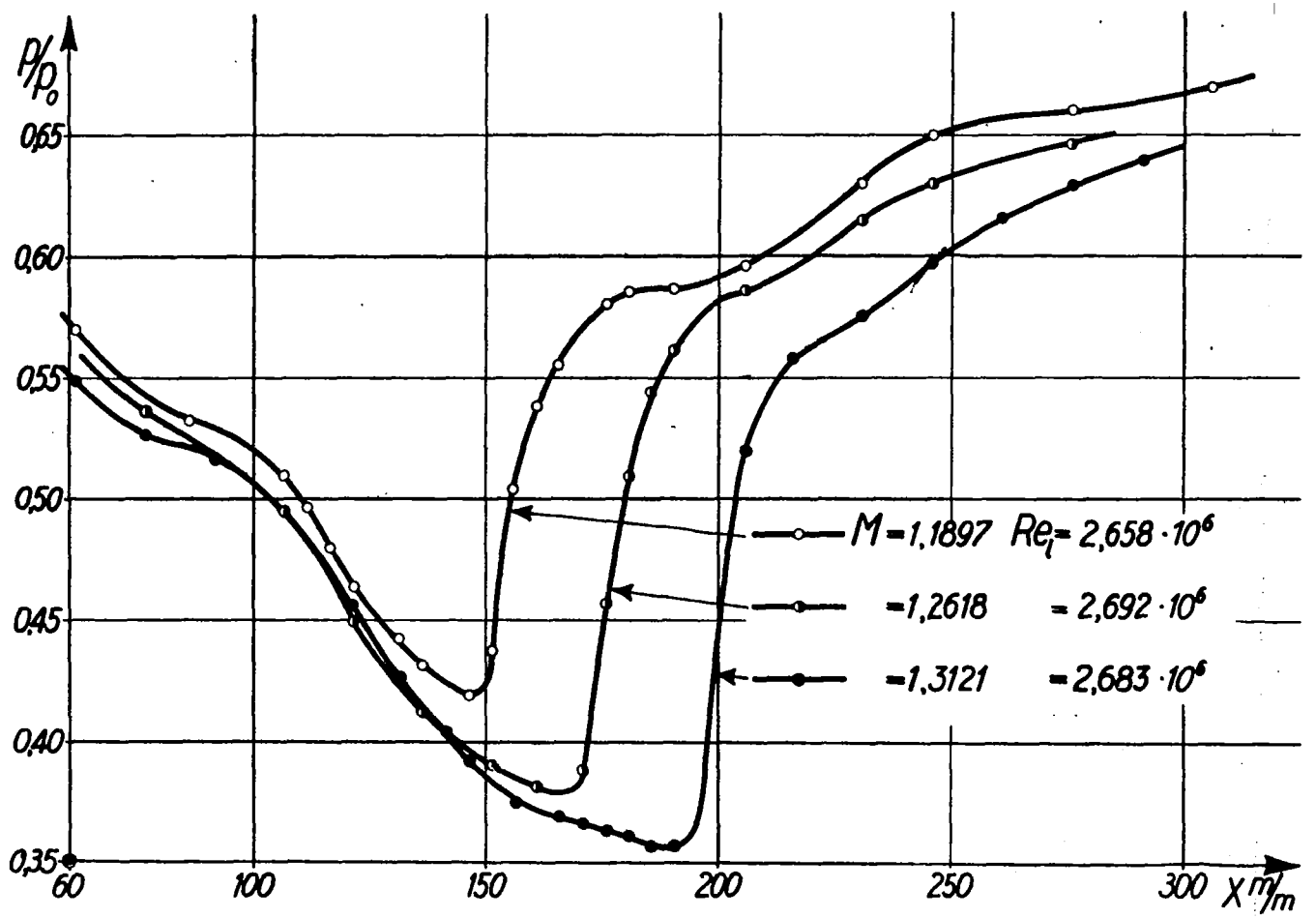

Figure 23.- Influence of the Mach number on the compression shock for turbulent boundary layer. Pressure distribution on the plate surface for 3 different Mach numbers.

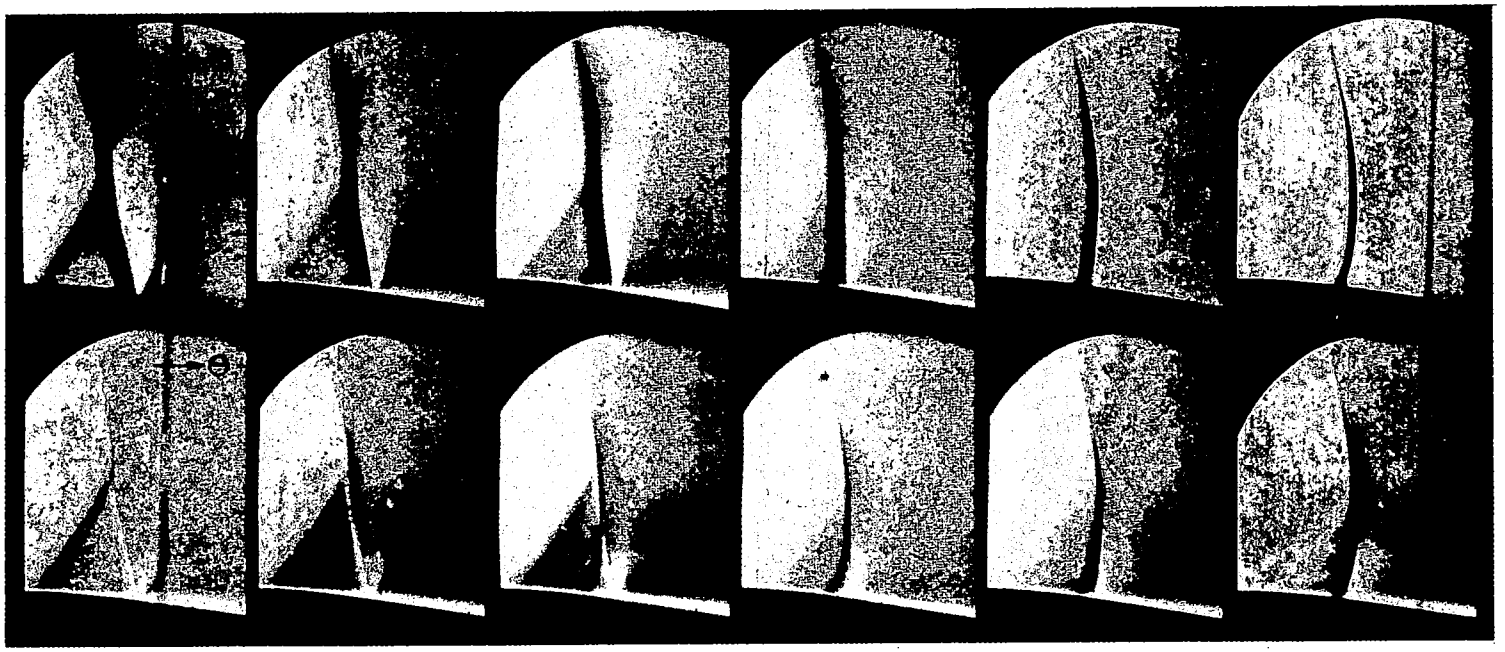

Re_l = 1.32 · 10^6 1.57 · 10^6 1.78 · 10^6 2.02 . 10^6 2.26 . 10^6 2.68 · 10^6

M = 1.22 M = 1.31

Figure 24.- Schlieren photograph. Influence of the Reynolds number on the compression shock for constant Mach number, of the free stream velocity with respect to the plate. Upper row: Schlieren knife-edge vertical. Lower row: Schlieren knife-edge horizontal.

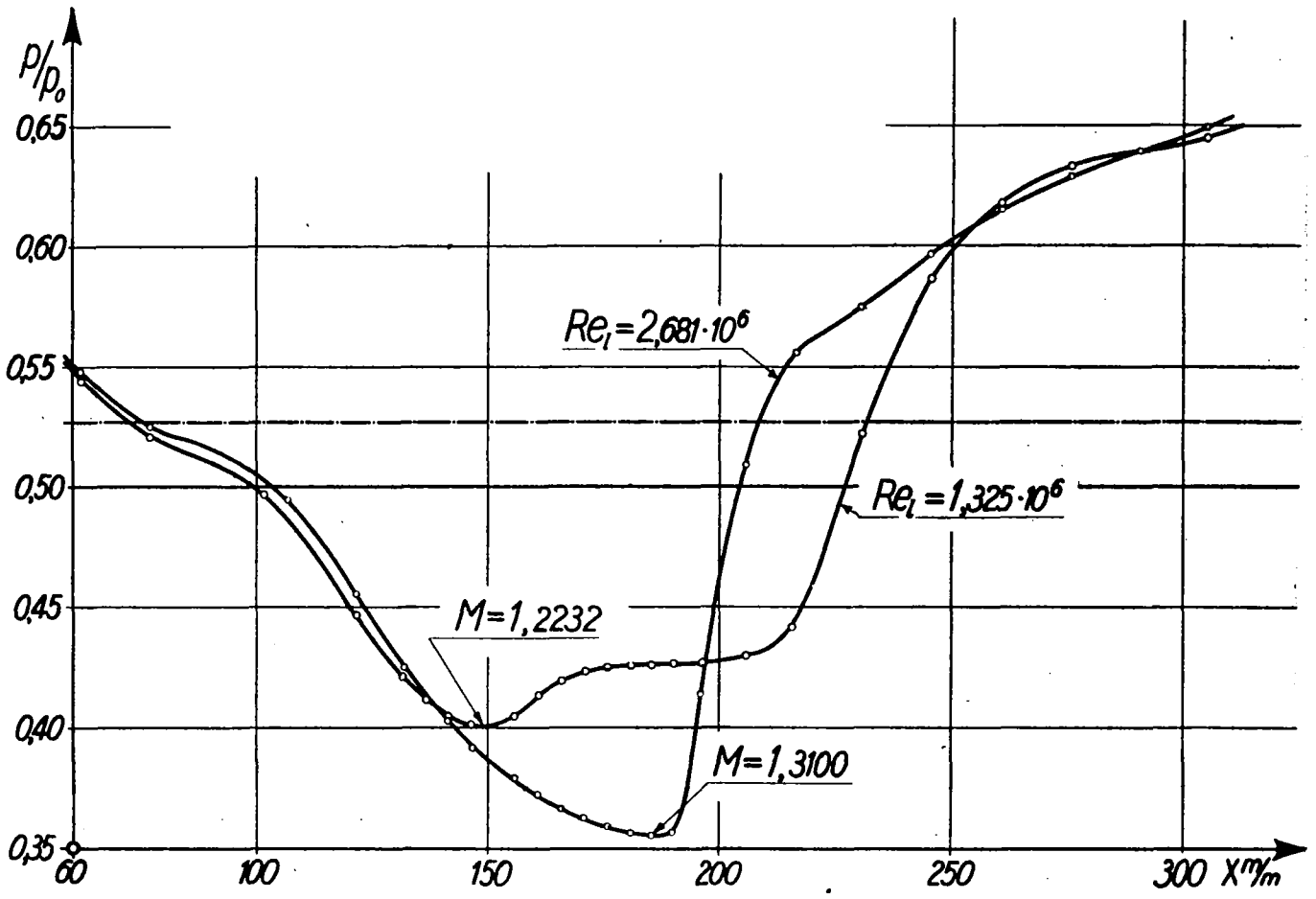

Figure 25.- Influence of the Reynolds number on the compression shock for constant Mach number, of the free stream velocity with respect to the plate. Pressure distribution at the plate surface.

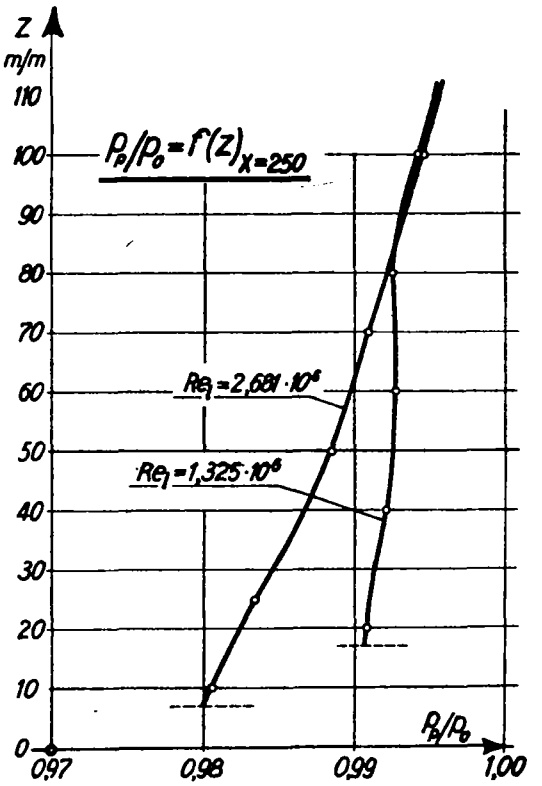

Figure 26.- Influence of the Reynolds number on the compression shock for constant Mach number of the free stream velocity with respect to the plate. Total pressure loss behind the compression shock.

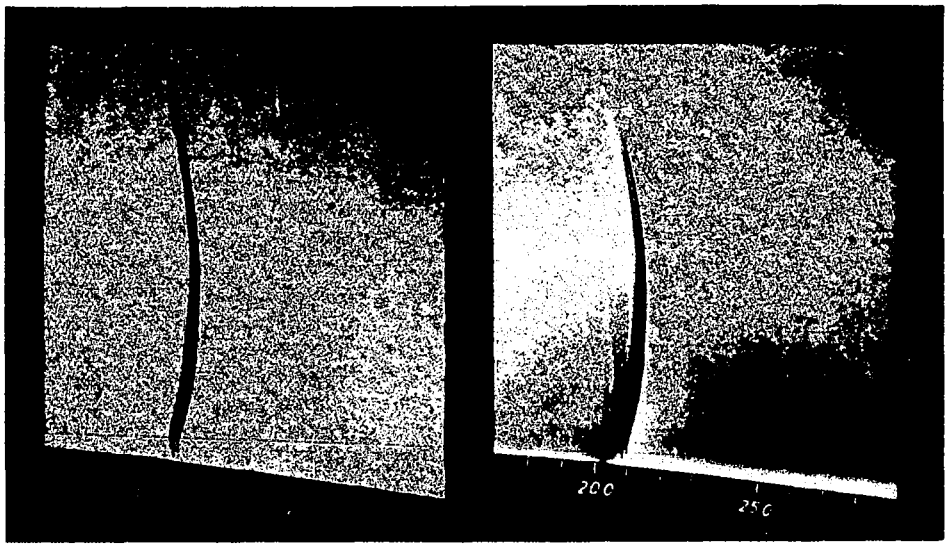

Figure 27.- Schlieren photograph. Turbulence wire ahead of the compression shock at the leading edge of the plate. $M = 1.28$, $Re_{\ell} = 1.69 \times 10^6$, $Re_{\delta}^{**} = 1159$.

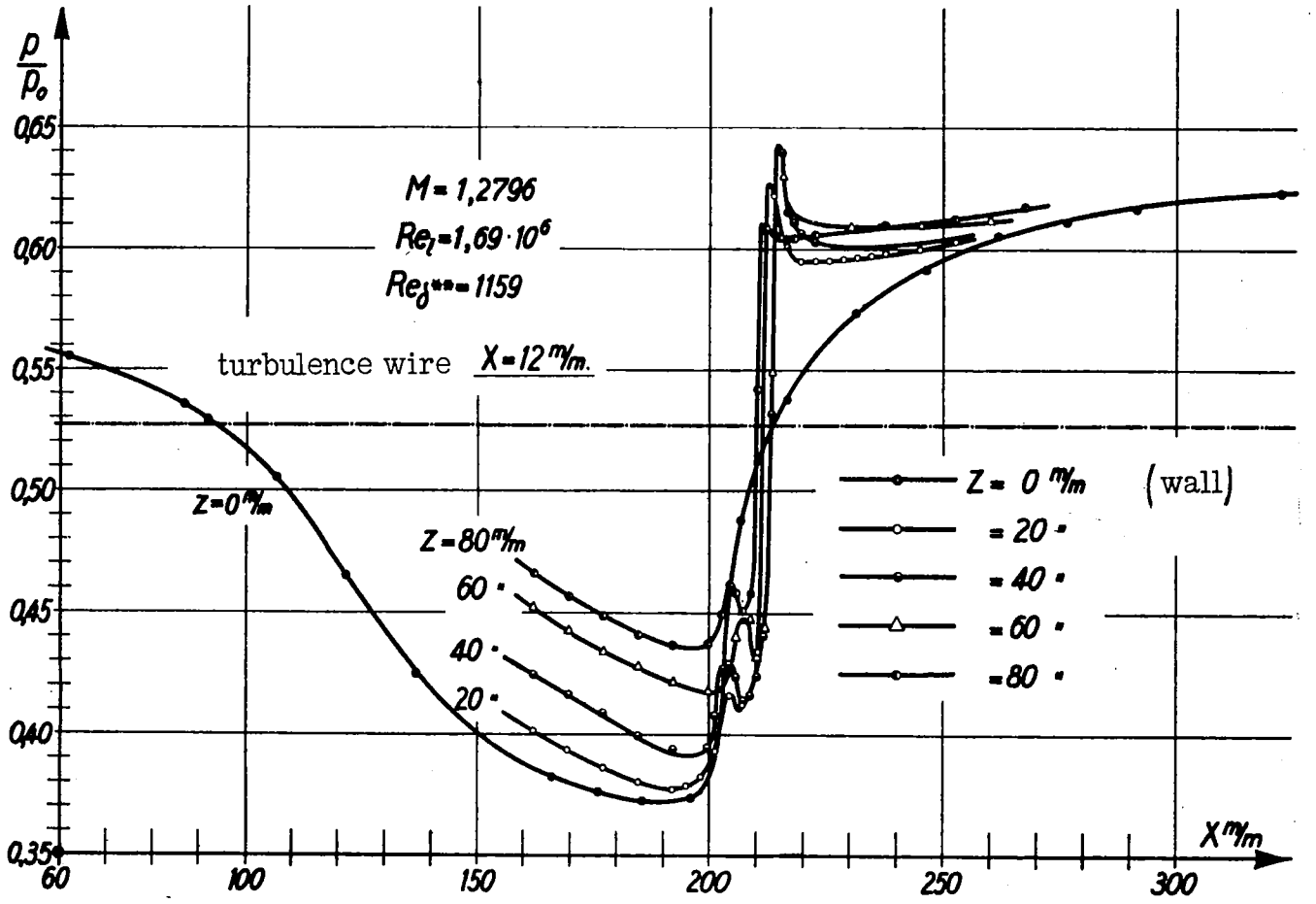

Figure 28.- Turbulence wire ahead of the compression shock at x = 12 mm. Distribution of the static pressure at various distances from the plate.

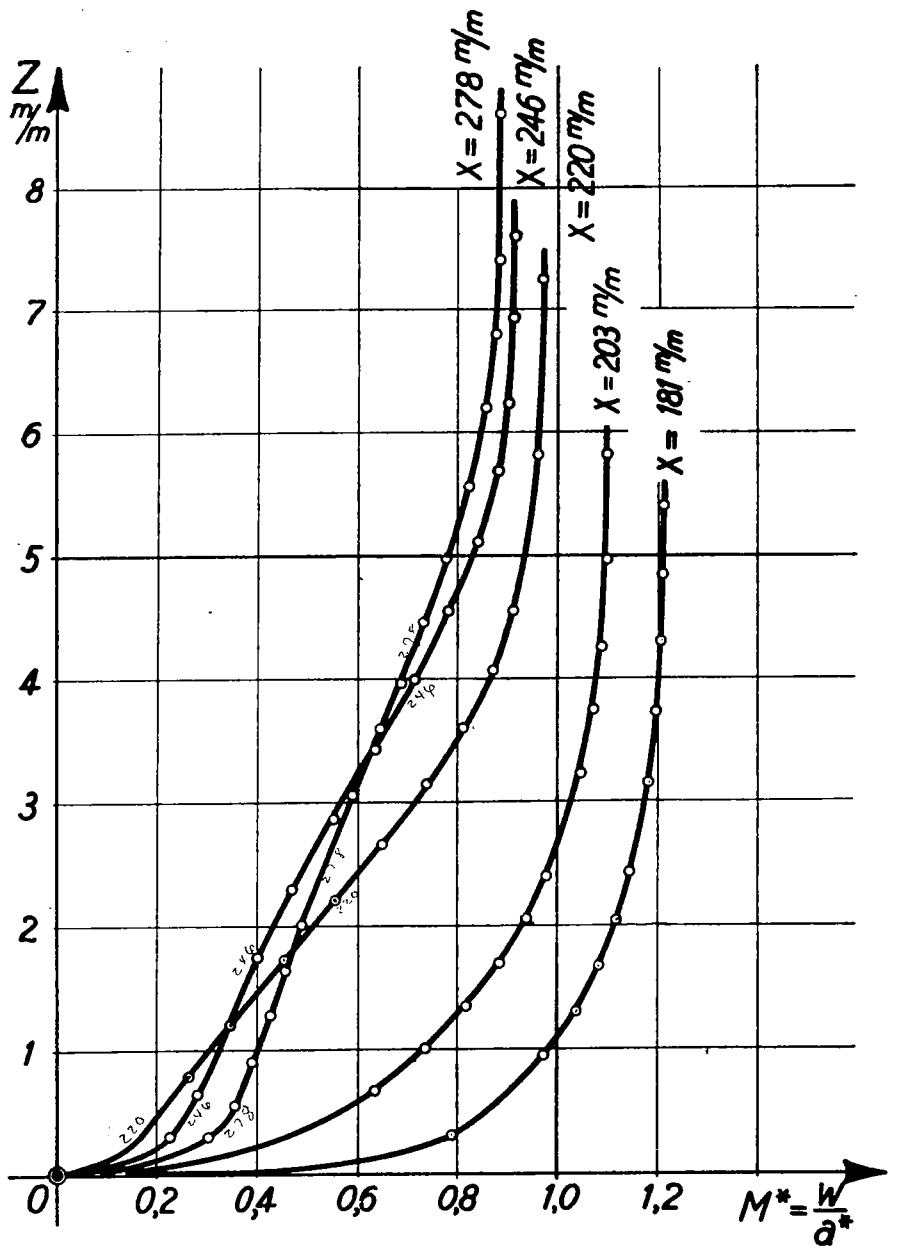

Figure 29.- Boundary layer profiles. $M^* = f(z)_x$. M = 1.279, $Re_l = 1.69 \times 10^6$, $Re_\delta{}^{**} = 1159$. Turbulence wire at x = 12 mm.

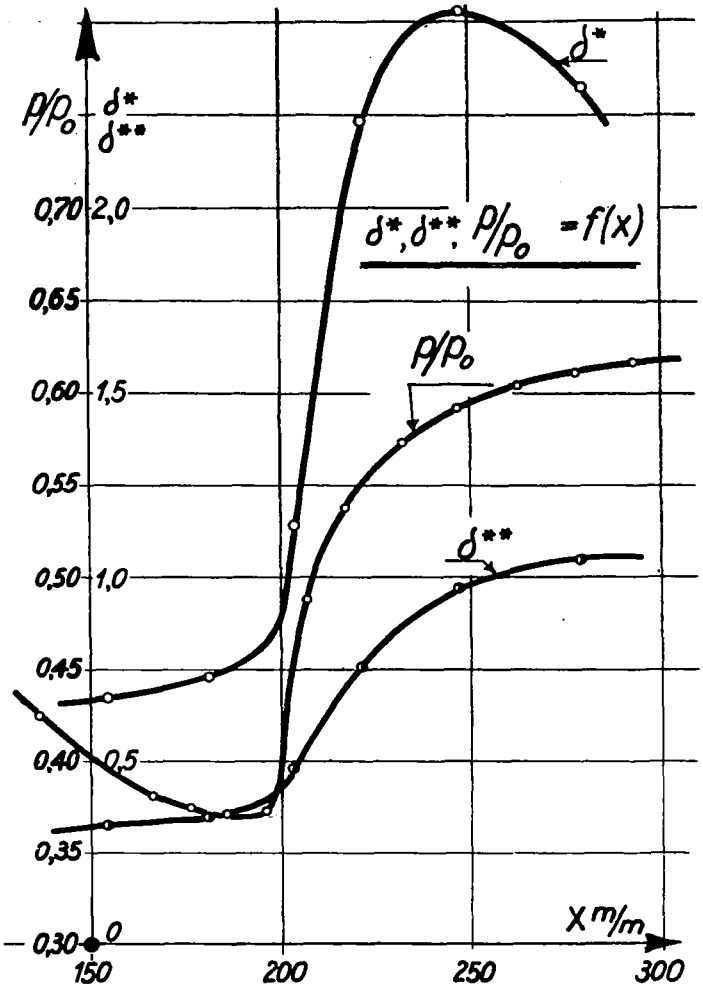

Figure 30.- Distribution of the displacement thickness δ^* and the momentum thickness δ^{**} of the boundary layer. M = 1.279, $Re_l = 1.69 \times 10^6$, $Re_{\delta^{**}} = 1159$. Turbulence wire at x = 12 mm.

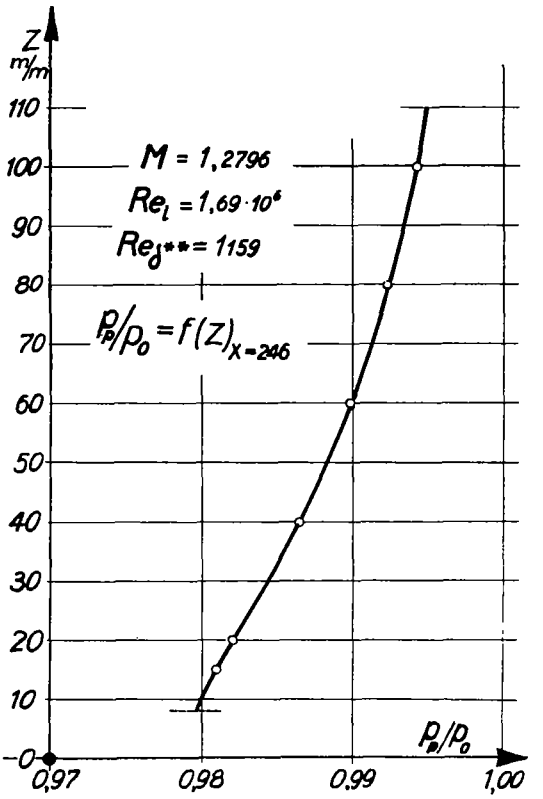

Figure 31.- Total pressure loss in the compression shock. Turbulence wire at x = 12 mm.

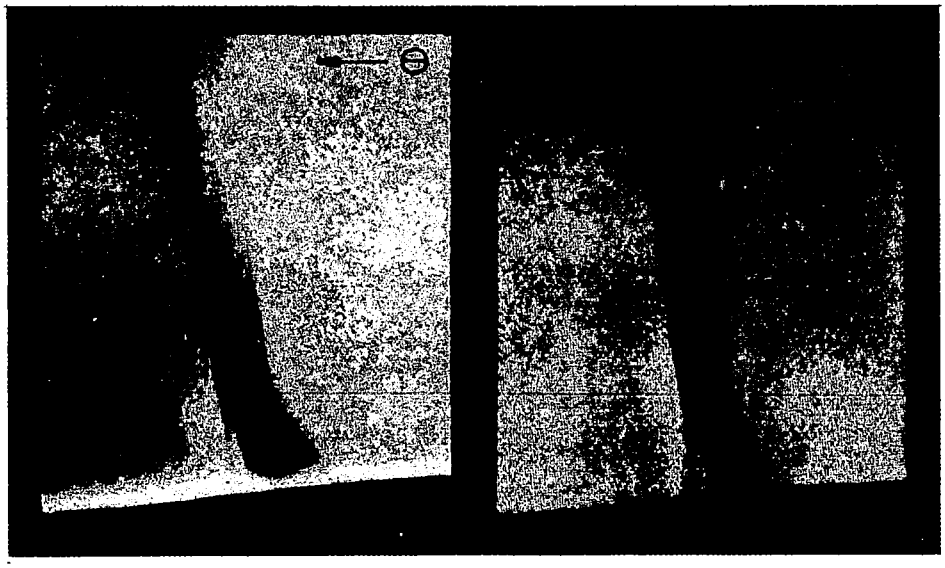

Figure 32.- Schlieren photograph. Compression shock for thick turbulent boundary layer. $M = 1.30$, $Re_{\delta^{**}} = 2315$.

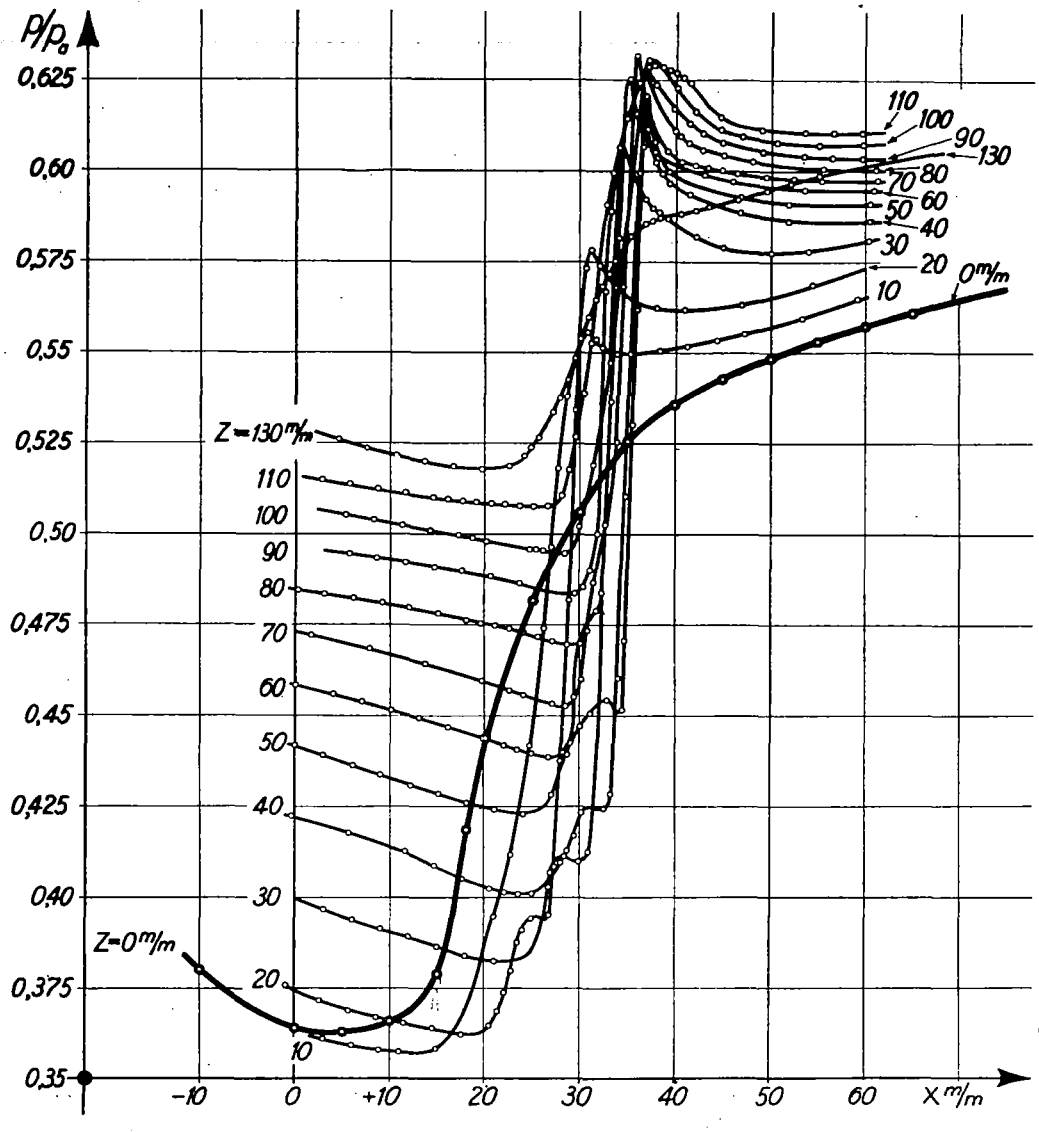

Figure 33.- Compression shock for thick turbulent boundary layer. M = 1.30, Re_{δ} ** = 2315. Distribution of the static pressure at various distances from the wall (x = 0 without auxiliary plate corresponds to x = 158 mm with auxiliary plate).

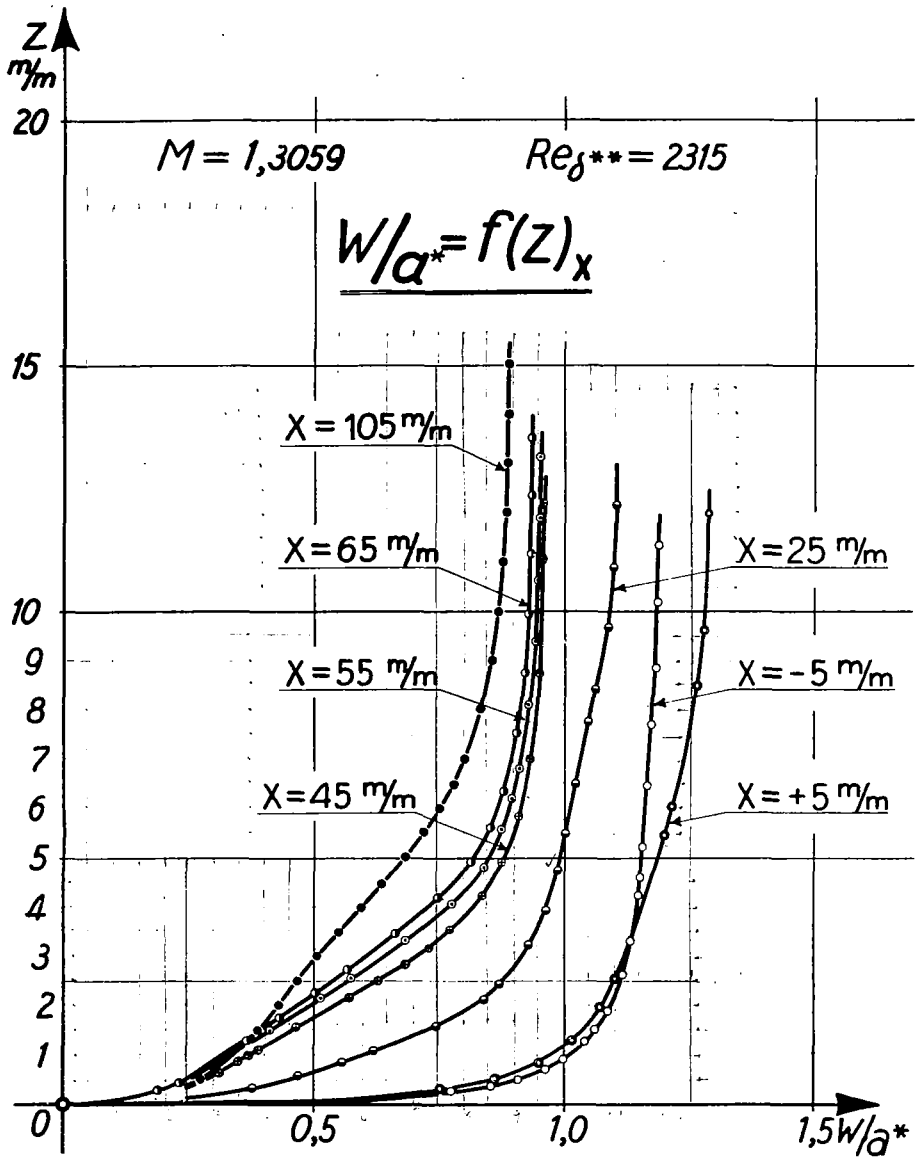

Figure 34.- Boundary layer profiles; $M^* = f(z)_x$.

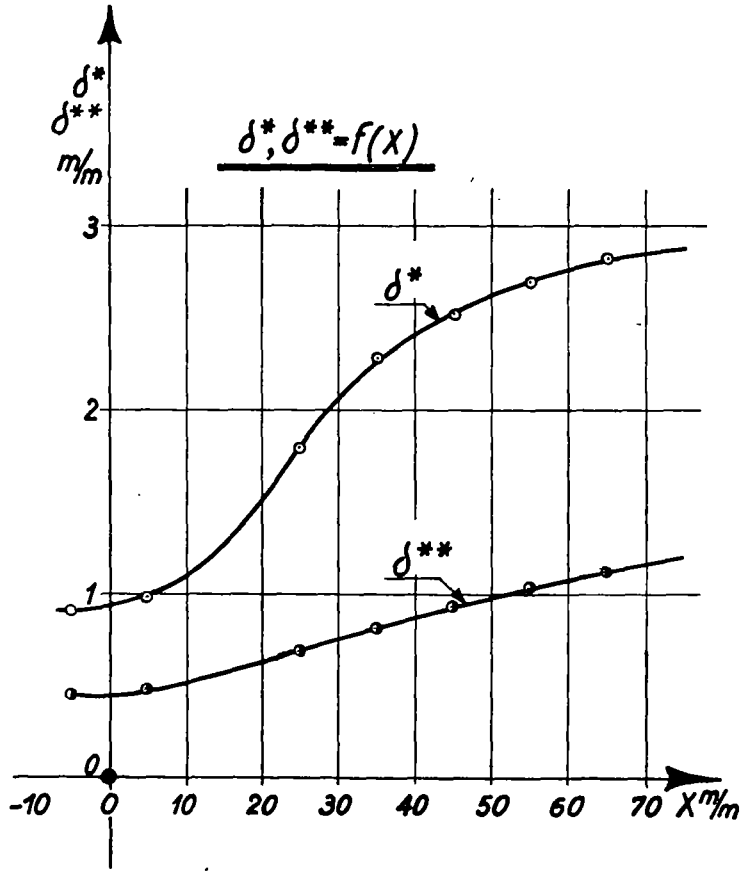

Figure 35.- Displacement thickness δ * and momentum thickness δ ** for the case of thick turbulent boundary layer in front of the shock. M = 1.30; Re_{δ} ** = 2315.

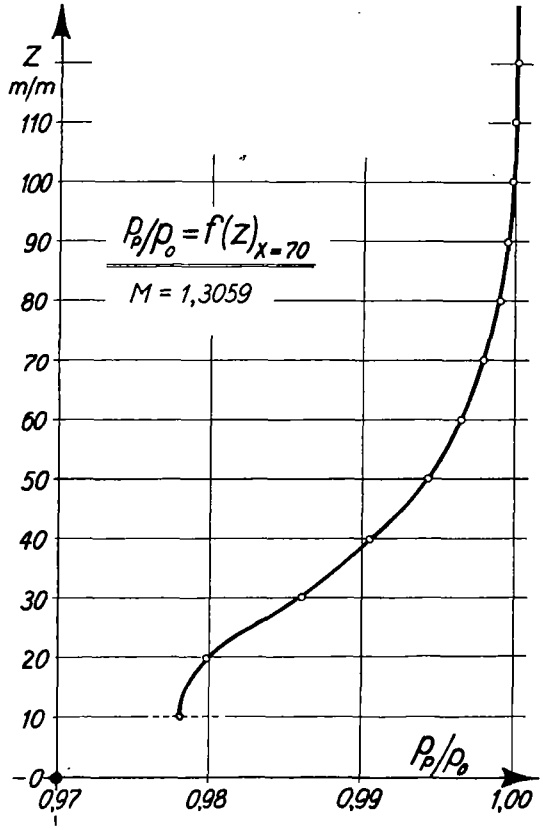

Figure 36.- Shock loss in the case of thick turbulent boundary layer in front of the compression shock. M = 1.30; Re_{δ} ** = 2315.

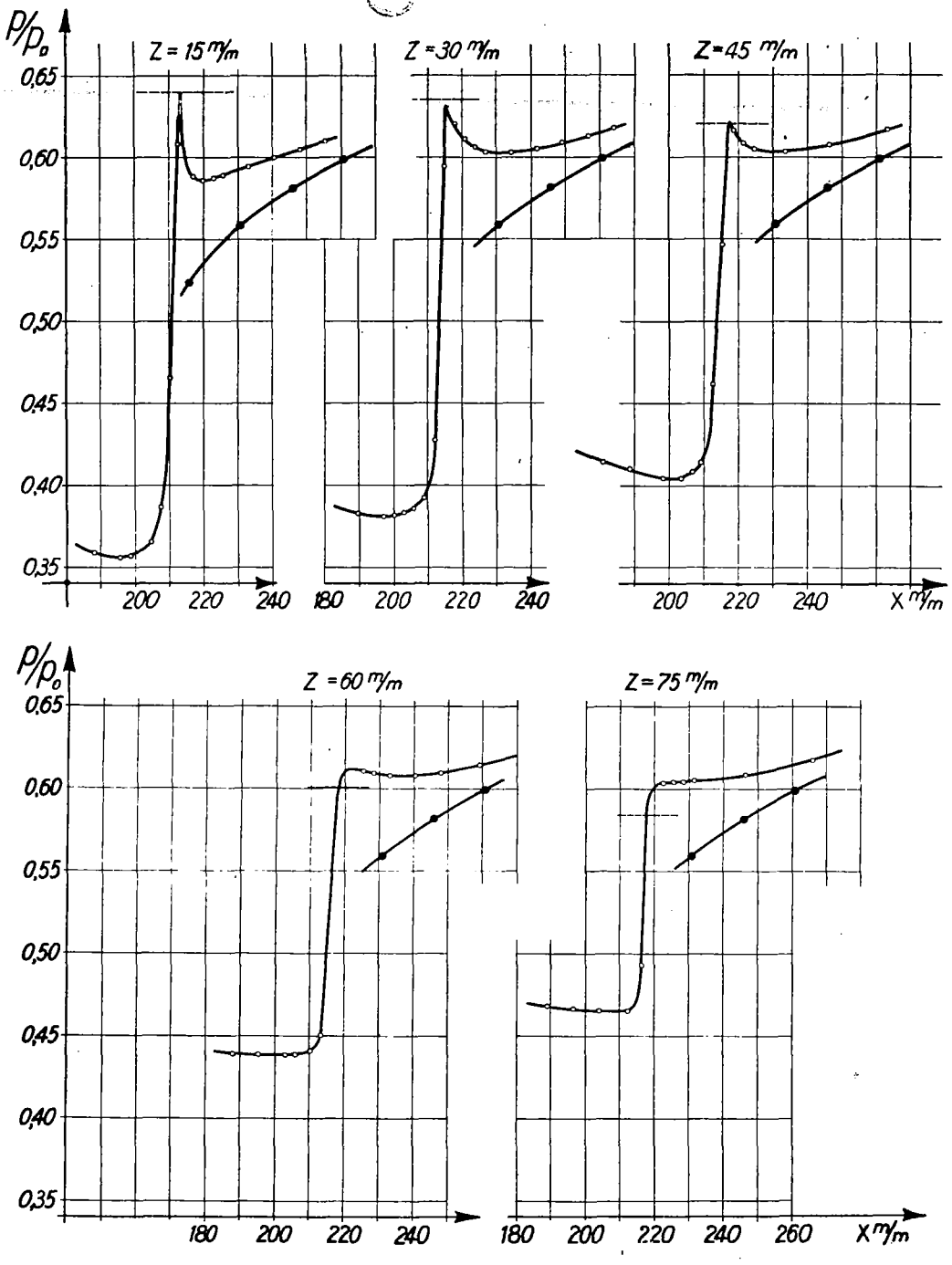

Figure 37.- Distribution of the static pressure through the shock at various distances from the plate. The dashed lines indicate the theoretical value of the final pressure in the compression shock. Segments of the pressure distribution on the plate surface are also plotted. (Solid dots).

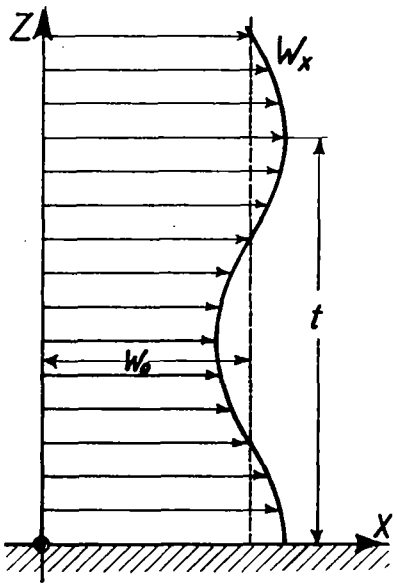

Figure 38.- Superimposed velocity distribution of the slightly disturbed parallel flow.

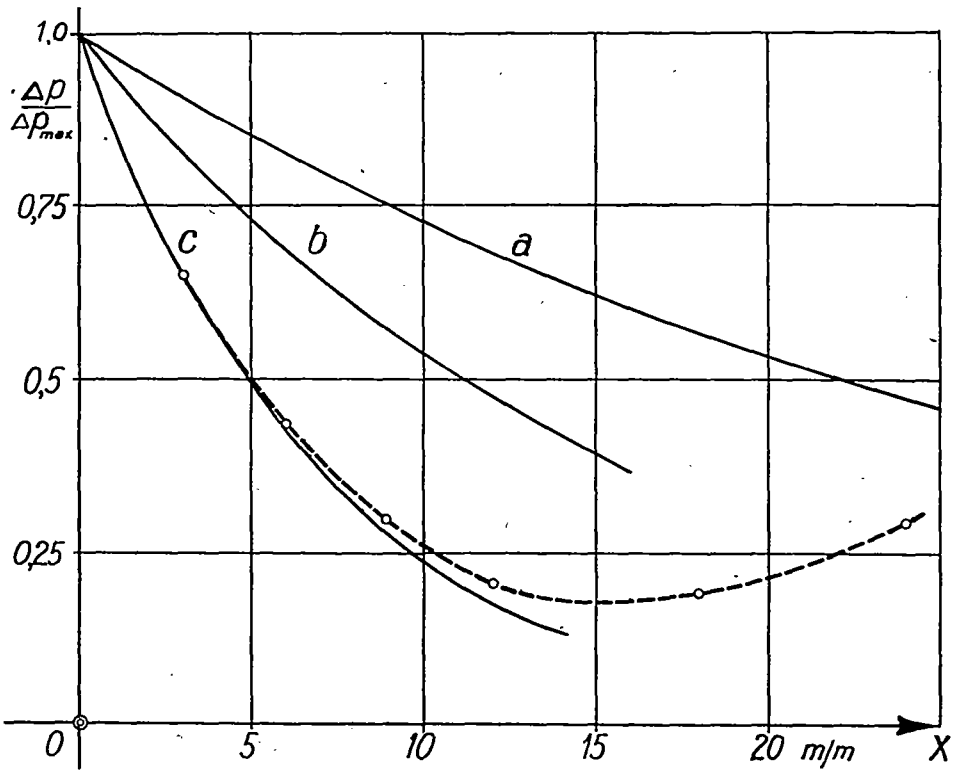

Figure 39.- Falling off of perturbations with the measured "wave length" $t^* \approx 200$ mm as basis. (a) exponential falling off for incompressible flow; (b) exponential falling off for compressible flow at the measured mean Mach number M = 0.87; (c) measured values with the most closely approximating exponential curve.

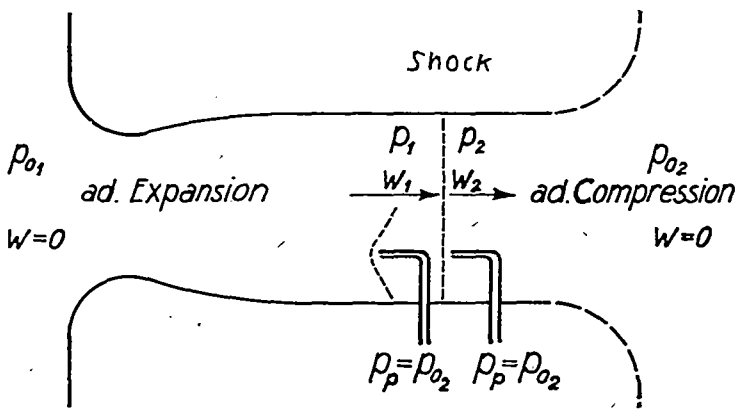

Figure 40.- Designation of the pressures at the normal compression shock.

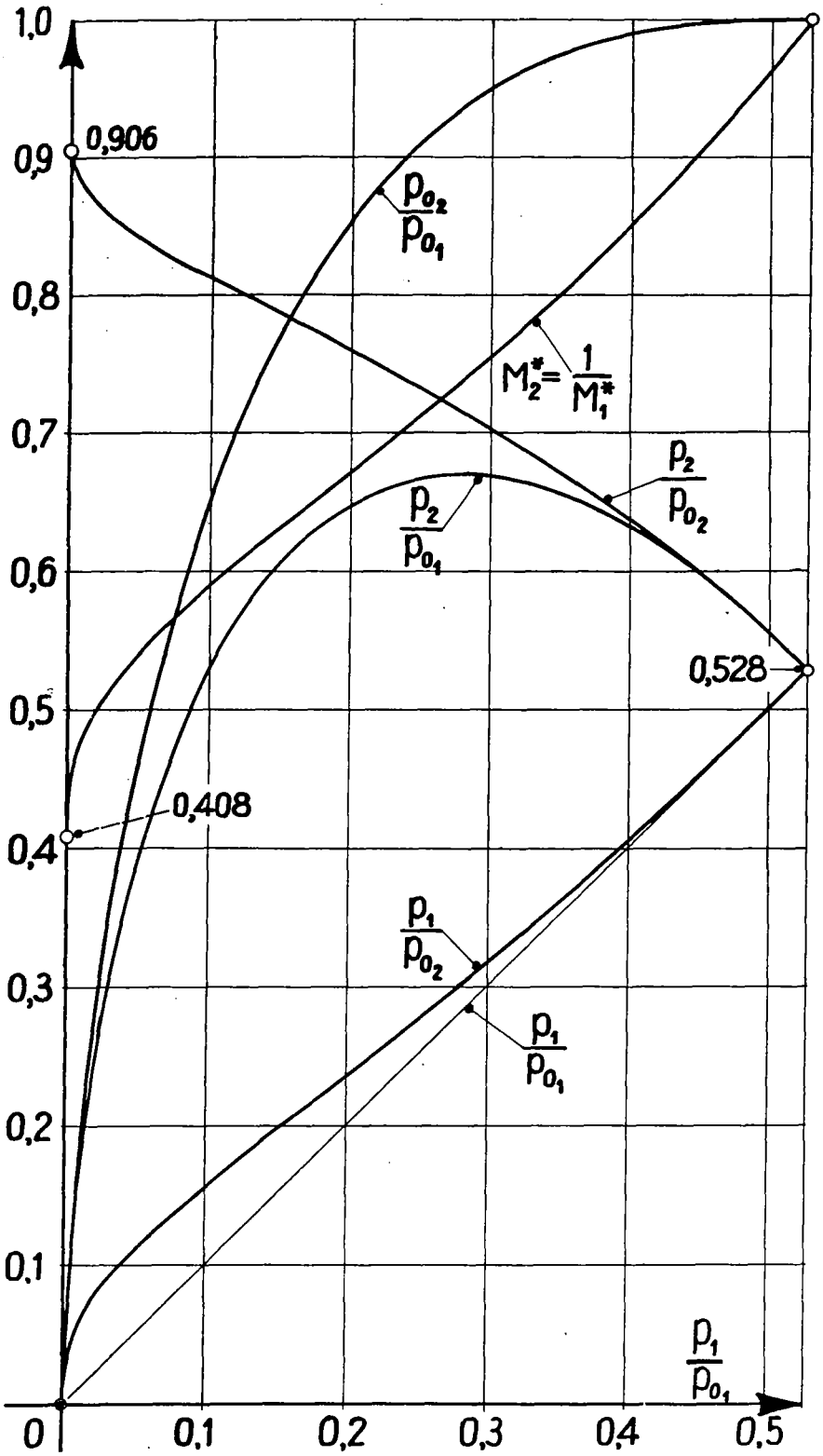

Figure 41.- Normal shock. k = 1.4.